

New Electron-Rich Diketiminolate Ligands: An Experimental and Computational
Investigation on the Isolation of Reactive Species

By
Michael Alexander Land

A Thesis Submitted to
Saint Mary's University, Halifax, Nova Scotia
in Partial Fulfillment of the Requirements for
the Degree of Bachelor of Science
with Honours in Chemistry.

April 2016, Halifax, Nova Scotia

Approved: Dr. Jason A.C. Clyburne
Supervisor
Department of Chemistry &
Environmental Science

Approved: Dr. Robert D. Singer
Chairperson
Department of Chemistry

Date: April 21, 2016

New Electron-Rich Diketiminato Ligands: An Experimental and Computational
Investigation on the Isolation of Reactive Species

Michael Alexander Land

Abstract

Boron analogues of NHCs have long eluded detection, likely due to their predicted low singlet-to-triplet energy gap. Two new *N,N'*-chelating ligands have been prepared and investigations into their reactivity and coordinative properties have started. A boron carbenoid that incorporates one of the new ligands has been probed computationally using both DFT and second-order Møller-Plesset methods. It has been found that the singlet state of this carbenoid is between 13.98 and 36.85 kJ mol⁻¹ more stable than its triplet state. To date, this is the only computationally investigated ligand system that stabilizes a neutral, six-membered heterocyclic, ground state singlet boron carbenoid. Attempts to prepare, and isolate, this compound have been unsuccessful, however, experimental evidence suggests further investigations should be made.

Organometallic complexes of the two new ligands have also been prepared and present interesting structural features. Rhodium carbonyl compounds have been synthesized with each ligand and these were studied to determine the ligands' electronic features, in comparison to each other and to the common 1,3-diketiminato (nacnac) ligand. It was found that one was experimentally identical to nacnac and the other had increased donor capabilities. A dimethylaluminum complex has also been prepared and both X-ray and DSC studies suggest that it assumes different solid state morphologies at various temperatures. Additionally, a long, Zn···C π -type interaction was observed in the corresponding ethylzinc complex.

April 21, 2016

Acknowledgements

First, I would like to thank my supervisor, Dr. Jason A.C. Clyburne. When I joined his research group over two years ago, I had no idea that chemistry, and research, would become a defining focus of my life. Since joining Jason's group I have had incredible opportunities and have achieved some amazing feats for which I am incredibly grateful and I cannot thank him enough.

I would also like to thank, and congratulate, my fellow Honours students, Zoe A. Paula, Bradley H.C. Green, and J. Kyle Awalt, for what we have accomplished this past year. The current and past members of Dr. Clyburne's research group, including ZAP, BHCG, R. Graeme Soper, Luke J. Murphy, and Juha Hurmalainen (who spent a year with us, from the University of Jyväskylä), have been great lab mates. Additionally, I would like to thank the best lab partner and friend, Angela D.K. Todd, for all of her assistance over the last four years. I'd also like to thank her supervisor, Dr. Jason D. Masuda, for allowing me to use his glovebox for the manipulation of moisture-sensitive compounds.

Dr. Katherine N. Robertson is someone else whom I cannot thank enough for everything that she has done during my time here. Her expertise with X-ray crystallography has led to a vast amount of the findings discussed within. She is also able to seamlessly handle multiple items and gives great advice which is always taken into consideration.

Although we have never met, I would like to thank Peter T.K. Lee for theorizing, and performing preliminary computations on the ligands discussed within, and Dr. Dragoslav Vidovic for proposing an early synthetic procedure for the preparation of the same ligand.

The Saint Mary's technicians, Elizabeth McLeod, Darlene Goucher, and Alyssa Doue, have been a great help while working in the chemistry department. Bright Huo, Jetsuda Areephong, and Iffenna I. Mbaezue were incredibly helpful during the summer of 2015, aiding in the preparation of the starting material, as well as performing the QTAIM analysis. I also thank ACEnet, the regional high performance computing consortium for universities in Atlantic Canada, for providing computational facilities and access to Gaussian.

Finally, I would like to thank Dr. Kai E.O. Ylijoki for everything he has taught me over the last three years. Although I no longer have classes with him, I still learn something from him almost daily. He is always willing to look over proposed organic syntheses, and give meaningful feedback. He has also taught me basic computational skills, and is someone with whom I hope to remain in contact as I continue in the field of chemistry. Without Dr. Ylijoki's assistance, a majority of this thesis would not have been possible.

“I love the lab – because it's all still magic”

- AMC's *Breaking Bad*

Table of Contents

Abstract	i
Acknowledgements	ii
Table of Contents	iii
List of Figures	v
List of Schemes	vi
List of Tables	vii
Table of Symbols and Abbreviations	viii
Chapter 1 – Introduction	1
1.1 Ligands and Coordination Complexes	1
1.2 Anionic <i>N,N'</i>-Chelating Ligands	2
1.3 <i>N</i>-Heterocyclic Carbenes	5
1.4 Main-Group Carbenoid Complexes	7
1.5 The Importance and Implications of a Boron-Based Carbene Analogue	13
1.6 Aim of this Thesis	15
Chapter 2 – Results & Discussion	16
2.1 Computational Optimizations of a New Ligand Designed for the Stabilization of a Carbene Analogue of Boron	16
2.2 Computational Investigations of the Optimized Boron Carbenoid	19
2.3 Experimental Ligand Preparation and Structural Investigations	21
2.4 Experimental Investigations of the Isolation of a Boron Carbenoid	26
2.5 Experimental Determination of the Electronic Donating Abilities of nocnoc and knicnac: The Preparation and Structural Investigation of Rhodium Carbonyl Complexes	28

2.6 Structural Investigation into the Reactions of NocNoc with Low-Coordinate Organometallic Reagents	33
2.7 Structural Investigation into the Reactions of KnicNac with Low-Coordinate Organometallic Reagents	41
Chapter 3 – Summary & Conclusions	44
Chapter 4 – Future Work	45
Chapter 5 – Experimental	46
5.1 General Procedures	46
5.2 Spectroscopic & Characterization Techniques	47
5.3 Gaseous HCl-free Synthesis of Diethyl Malonimidate Dihydrochloride	49
5.4 Synthesis of NocNoc, 2	50
5.5 Synthesis of KnicNac, 3	51
5.6 Deuterium Exchange Study	52
5.7 Synthesis of the Rhodium Carbonyl Complex of nocnoc, 4	52
5.8 Synthesis of the Rhodium Carbonyl Complex of knicnac, 5	53
5.9 Synthesis of the Dimethylaluminum Complex of nocnoc, 6	54
5.10 Synthesis of the Ethylzinc Complex of nocnoc, 7	55
5.11 Synthesis of <i>Bis</i> (knicnac)zinc, 8	55
5.12 Computational Details	56
5.13 X-ray Crystallographic Details	58
References	61
Chapter 6 – Appendix	69
6.1 Computational Data	69
6.2 Crystallographic Data	71

List of Figures

Figure 1: Structures of the <i>N,N'</i> -chelating ligands discussed herein.	2
Figure 2: Space-filling model of 1,3- <i>bis</i> (2,4,6-trimethylphenyl)imidazole-2-ylidene as an example for the “bowl-shaped” pocket.	3
Figure 3: Group 13 carbene analogues isolated to date.	8
Figure 4: Solid state structure of the first aluminum carbene analogue.	9
Figure 5: Crystal structure of the boryllithium-DME dimer reported by Nozaki <i>et al.</i>	11
Figure 6: General structure of the boron carbenoid to be optimized.	16
Figure 7: Graphical representations of Entry 1 and Entry 5 from Table 2.	18
Figure 8: Graphical representations of 1s .	20
Figure 9: HOMO, LUMO, and the electrostatic potential map of 1s .	21
Figure 10: Solid state structure of NocNoc, 2 .	24
Figure 11: Solid state structure of KnicNac, 3 .	25
Figure 12: Resonance structures of the anionic <i>N,N'</i> -chelating ligands.	26
Figure 13: <i>d-π*</i> backbonding in a metal carbonyl compound.	29
Figure 14: Solid state structures of the rhodium dicarbonyl compounds 4 and 5 .	30
Figure 15: Graphical representation of the “puckering” observed in 5 .	31
Figure 16: Solid state structure of the dimethylaluminum complex of nocnoc, 6 .	35
Figure 17: Solid state structures of 6 at 125 K and 298 K.	35
Figure 18: DSC curve of 6 .	36
Figure 19: Solid state packing of 6 .	38
Figure 20: Solid state structure of the ethylzinc complex of nocnoc, 7 .	39
Figure 21: Bond critical points in the dimeric structure of 7 .	41
Figure 22: Solid state structure of <i>bis</i> (knicnac)zinc, 8 .	43
Figure A1: Graphical representation of 1D .	70
Figure A2: Graphical representation of the dipole in 6 .	70
Figure A3: Ring contacts present in the solid state structure of 2 .	71
Figure A4: Large, “block-like” crystal of 6 .	71
Figure A5: Solid state dimeric structure of 7 .	72

List of Schemes

Scheme 1: Formation of the coordination complex, <i>tris</i> (acetylacetonato)iron (III).	1
Scheme 2: Synthesis of the 1,3-diketiminato, NacNac, and its enamine tautomer.	4
Scheme 3: Deprotonation at the β -position of nacnac.	4
Scheme 4: The biosynthesis of furoin from furfural.	5
Scheme 5: Synthesis of an <i>N</i> -heterocyclic carbene.	6
Scheme 6: Synthesis of the first neutral, Group 13 carbene analogue.	8
Scheme 7: Synthesis of the boron-containing products that incorporated a “trapped” boron carbenoid.	13
Scheme 8: Theoretical C–H bond activation of pentane <i>via</i> low-valent boron.	14
Scheme 9: The preparation of the first imidazol-2-carboxylate and the predicted boron carbenoid reactivity with CO ₂ .	15
Scheme 10: Gaseous HCl- <i>free</i> synthesis of diethyl malonimidate dihydrochloride.	22
Scheme 11: Synthesis of diethyl- <i>N,N'</i> - <i>bis</i> (<i>p</i> -tolyl)malonimidate, 2 , NocNoc.	23
Scheme 12: Proposed mechanism for the formation of DEMHCl and NocNoc.	23
Scheme 13: Synthesis of 1,3- <i>bis</i> (dimethylamino)- <i>N,N'</i> - <i>bis</i> (<i>p</i> -tolyl)propanediimidate, 3 , KnicNac.	25
Scheme 14: Determination of the relative acidity of the ligand precursors at the α -position <i>via</i> deuterium exchange.	26
Scheme 15: Retrosynthetic analysis of the boron carbenoid, 1s .	27
Scheme 16: Synthetic route to the rhodium dicarbonyl compounds, 4 and 5 .	30
Scheme 17: Resonance structure of the Lewis acid explicitly showing its carbanion.	33
Scheme 18: Synthesis of the dimethylaluminum complex of nocnoc, 6 .	34
Scheme 19: Synthesis of the ethylzinc complex of nocnoc, 7 .	39
Scheme 20: Synthesis of <i>bis</i> (knicnac)zinc, 8 .	42

List of Tables

Table 1: Calculated singlet-triplet energy gaps and the relative energies for the dimerization process for the Group 13 carbenoids of nacnac.	10
Table 2: Modifications of R ¹ to obtain the largest singlet-triplet gap.	18
Table 3: Modifications of R ² to obtain the largest singlet-triplet gap.	19
Table 4: Experimentally determined, and calculated, spectroscopic values corresponding to the carbonyl groups.	32
Table A1: Energy output for the optimization of the R ¹ position.	69
Table A2: Energy output for the optimization of the R ² position.	69
Table A3: Summary of computed energy data for the optimized boron carbenoid.	69

Table of Symbols and Abbreviations

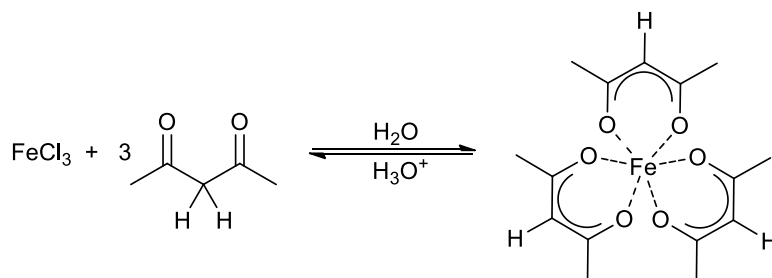
°	degrees
°C	degrees Celsius
ΔE_{st}	singlet-to-triplet energy gap
ΔG_{D}	Gibbs free energy of the dimer, relative to the starting materials
ΔH_{D}	enthalpy of dimerization
δ_{CO}	carbonyl chemical shift
ν_{CO}	carbonyl stretching frequency
Å	Angstrom (10^{-10} m)
<i>ab initio</i>	from Latin, meaning “from the beginning”
AIM	atoms in molecules
AlMe ₃	trimethylaluminum
Ar	aryl
ATR	attenuated total reflection
B	Brønsted base
B3LYP	Becke, three-parameter, Lee-Yang-Parr hybrid functional
BCP	bond critical point
BOX	<i>bis</i> (oxazoline) ligand
br	broad
C ₆ D ₆	deuterated benzene
<i>ca.</i>	<i>circa</i> (from Latin, meaning “about, approximately”)
CCDC	Cambridge Crystallographic Data Centre
CO ₂	carbon dioxide
<i>et al.</i>	<i>et alii</i> (from Latin, meaning “and others”)
cm ⁻¹	wavenumber
D ₂ O	deuterium oxide
DAB	1,4-diaza-1,3-butadiene
DCM	dichloromethane
dec	decomposition
DEMHC1	diethyl malonimidate dihydrochloride
DFT	density functional theory
Dipp	2,6-diisopropylphenyl
DME	1,2-dimethoxyethane
DMSO-D ₆	deuterated dimethylsulfoxide
DSC	differential scanning calorimetry
EA	elemental analysis
EDG	electron donating group
Et ₂ Zn	diethylzinc
eV	electronvolt
g	gram
Ha	hartree
HOMO	highest occupied molecular orbital
HRMS	high-resolution mass spectrometry
<i>in situ</i>	from Latin, meaning “in the reaction mixture”

<i>in vacuo</i>	from Latin, meaning “in a vacuum”
IR	infrared
<i>J</i>	coupling constant
K	kelvin
KC ₈	potassium-graphite
kJ mol ⁻¹	kilojoule per mole
KnicNac	1,3- <i>bis</i> (dimethylamino)- <i>N,N'</i> - <i>bis</i> (<i>p</i> -tolyl)propanediimidate
knicnac	deprotonated, anionic ligand of KnicNac
LUMO	lowest occupied molecular orbital
M	molar (moles per liter)
m	multiplet/medium
Mes	mesityl
MHz	megahertz
mL	milliliter
mmol	millimole
mp	melting point
MP2	second order Møller-Plesset perturbation theory
NacNac	1,3-diketiminato ligand precursor (also known as HNacNac)
nacnac	deprotonated, anionic ligand of NacNac
NocNoc	diethyl- <i>N,N'</i> - <i>bis</i> (<i>p</i> -tolyl)malonimidate
nocnoc	deprotonated, anionic ligand of NocNoc
NHC	<i>N</i> -heterocyclic carbene
NMR	nuclear magnetic resonance
Ph	phenyl
PM3	parameterized model number 3, semi-empirical method
ppm	parts per million
<i>p</i> -tol	4-tolyl
q	quartet
REDOX	reduction-oxidation
s	singlet/strong
t	triplet
<i>t</i> -Bu	<i>tert</i> -butyl
THF	tetrahydrofuran
vs	very strong
W	watt (J s ⁻¹)
w	weak

Chapter 1 – Introduction

1.1 Ligands and Coordination Complexes

In chemistry, metal cations are generally considered to be Lewis acids. This means that they can accept a pair of electrons from a Lewis base, resulting in the formation of a Lewis adduct. In organometallic chemistry, this product is referred to as a coordination complex as the metal centre forms *coordinate bonds* with a Lewis base (Scheme 1).¹ The coordinating Lewis bases that will be discussed herein are also known as ligands, a word which comes from the Latin verb, '*ligare*' meaning 'to bind'.¹ A majority of the ligands generally found in inorganic chemistry are neutral, such as water, phosphines, ethers, amines, and carbenes, which will be discussed later. While the neutral ligands listed are some of the most common, they are not the only type of ligand. Ligands can also be anionic, which may be the type that are most commonly found in coordination complexes. Although much less common, ligands can also be cationic, such as the *bis*(arylamino)phosphenium cations reported by Baker *et al.*^{2,3} Other than by charge, ligands can also be classified by how many atoms they contain that are capable of forming a coordinate bond. Ligands that coordinate to a metal centre through only a single atom are termed monodentate, while ligands that are bi- and tridentate chelate through two and three atoms, respectively. It should also be noted that charge does not dictate denticity.



Scheme 1: Formation of the coordination complex, *tris*(acetylacetonato)iron (III).

1.2 Anionic N,N' -Chelating Ligands

As previously mentioned, some of the most studied ligands are anionic. The chloride anion is such an anionic ligand as it occupies a coordination site, however, compared to other ligands discussed herein, it is not very interesting. Since the end of the metallocene era, bulky nitrogen chelating ligands have replaced the common η^5 -cyclopentadienyl ligand for the stabilization of reactive species. One type of N,N' -chelating ligand which has been investigated, although not the focus of this thesis, are the guanidinate ligands, **I**. Guanidinate ligands are monoanionic ligands that can chelate through both nitrogen atoms; they are capable of forming either bidentate or bridging structures.⁴ While it has been shown that guanidinate ligands have applications for the stabilization of low-valent species, which will be described in a later section, the ligands themselves do not directly relate to the discussions presented later in this thesis and therefore the structural characteristics of these ligands will not be discussed in further detail.

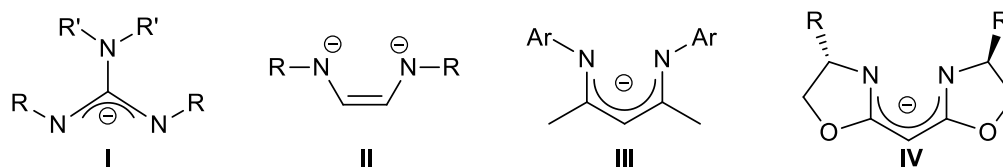


Figure 1: Structures of the N,N' -chelating ligands discussed herein ($R, R' = \text{aryl, alkyl}$).

Another common reagent that has been widely used as an N,N' -chelating ligand over the last 40 years is 1,4-diaza-1,3-butadiene (DAB), **II**.⁵ Generally, this is a dianionic ligand that can easily form five-membered ring systems. The two most common substituents found on DAB are *t*-butyl and 2,6-diisopropylphenyl (Dipp). These bulky substituents form a “bowl-shaped” pocket that is capable of providing an unique environment (Figure 2),⁶ which can facilitate novel chemistry by the stabilization of reactive species. One of the notable features of DAB is that it has the same structural back-bone (NCCN) as

N-heterocyclic carbenes, which will be discussed in detail in the following section. It is because of this feature that this ligand is even described in this thesis, however, as will also be described later, the employment of a dianionic ligand is not always ideal.

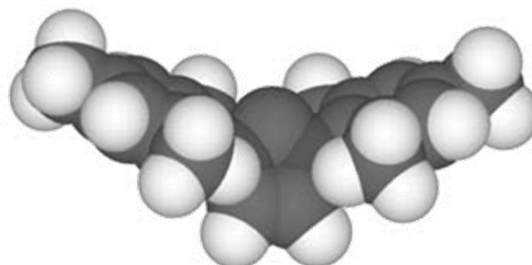
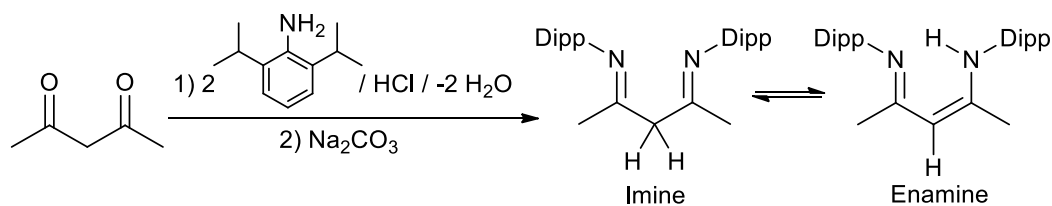


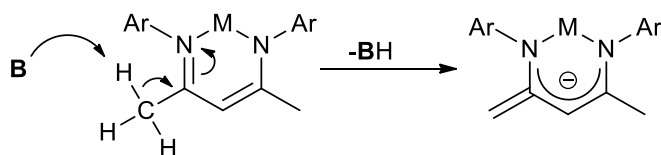
Figure 2: Space-filling model of 1,3-*bis*(2,4,6-trimethylphenyl)imidazole-2-ylidene as an example for the “bowl-shaped” pocket described above. Adapted from Ref. 6 with permission from The Royal Society of Chemistry.

In 1997 Feldman *et al.*⁷ reported a new ligand (Scheme 2) which has since been extensively used in a wide range of applications. This ligand, that the authors called nacnac due to its similarity to the common acac ligand, is also a bidentate, *N,N'*-chelating ligand with bulky Dipp substituents. Generally, the term NacNac (or HNacNac) is used to describe the ligand precursor, whereas the deprotonated 1,3-diketiminato ligand, **III**, is known as nacnac. This ligand has been shown to be REDOX active,⁸ and has been incorporated into many organometallic complexes.⁹ Complexes of nacnac have been shown to be effective for: the catalysis of ethene polymerization,⁹⁻¹¹ the isolation of biomimetic intermediates,¹² and for the catalytic reduction of CO₂,¹³ where it forms a derivative of methanol. These are just a few, of the many, examples in which nacnac has been used; see the accompanying references for full reviews on the topic.^{8,9} The reactivity of the ligand precursor is likely driven by the presence of its tautomeric form; similar to keto-enol tautomerization, NacNac can undergo imine-enamine tautomerization, with the enamine being favoured (Scheme 2).



Scheme 2: Synthesis of the 1,3-diketiminato, NacNac, and its enamine tautomer.

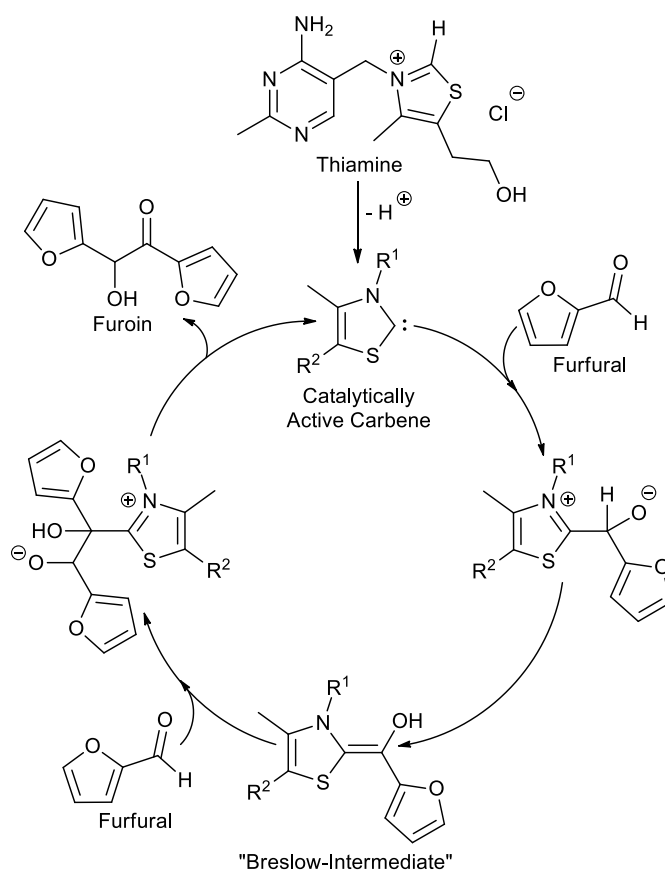
The nacnac ligand, and variations of it, have been implemented into many organometallic complexes, with a wide array of applications, especially in the field of catalysis. Many catalytic reactions, primarily those involved in the formation of carbon-carbon bonds, require relatively harsh conditions. Due to this, it is important to use robust ligands when preparing catalysts, such that, the catalysts do not undergo degradation. It has been shown that nacnac is a non-innocent ligand,¹⁴ and it can undergo deprotonation at the β -position in the presence of a strong Brønsted base (Scheme 3).¹³⁻²⁰ This results in the formation of a methylene carbon whose negative charge is then delocalized throughout the entire framework of the ligand. This is not a desirable characteristic of a catalyst as it can deactivate it, effectively rendering it useless. There is another N,N' -chelating ligand whose substitution prevents this deprotonation from occurring. The *bis*(oxazoline) (BOX) ligands, **IV**, have an alkoxy group in the β -position which increases their stability, compared to nacnac, under harsh conditions. One of the main applications of BOX type ligands is for asymmetric catalysis in Diels-Alder reactions.²¹ Since BOX ligands can form chiral molecules, the aryl substituents cannot assume the correct geometry to form the desired “bowl-shaped” pocket.



Scheme 3: Deprotonation at the β -position of nacnac in the presence of a strong base (M = metal centre, B = Brønsted base).

1.3 *N*-Heterocyclic Carbenes

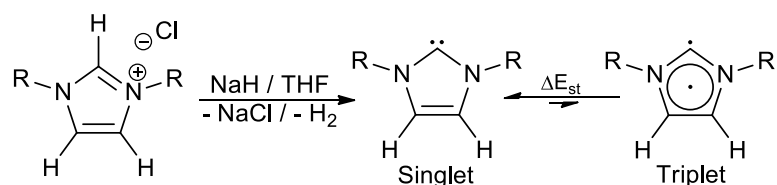
The benzoin condensation reaction, first reported by Wöhler and Liebig in 1832,²² is similar to a key biological process in which two aromatic aldehydes are combined to form aromatic acyloins. Wöhler and Liebig employed cyanide as a catalyst; however, the coenzyme thiamine (vitamin B₁) is responsible for the generation of acyloin-like compounds in many biochemical systems (Scheme 4).²³ In 1958 Breslow proposed that the catalyst responsible for the biosynthesis of furoin, from furfural, was a nucleophilic carbene derivative, formed from thiamine during the catalytic cycle;²⁴ this “Breslow-intermediate” was not isolated in the solid state until 2012.²⁵



Scheme 4: The biosynthesis of furoin from furfural, a component of vanilla.

One of the goals of synthetic main group chemists is to isolate highly reactive compounds by preparing novel bonding frameworks to stabilize these species. A class of

these highly reactive species, which has had a significant impact on the fields of organic and inorganic chemistry since one was first prepared as an isolable solid in 1991 by Arduengo *et al.*,^{26,27} is the *N*-heterocyclic carbene (NHC).²⁸ Carbenes are neutral molecules that contain an electron deficient, divalent carbon atom, making them some of the most (Brønsted) basic compounds known.^{29,30} Highly reactive alkyl carbenes have traditionally been used in organic chemistry, however, these are generated *in situ*, and have not been isolated in the solid state. This high reactivity results because the triplet state is favoured, and therefore carbenes eluded isolation for many years as it requires a combination of steric and electronic effects to stabilize them in the solid state.^{26,27} The first NHC was prepared by the deprotonation of the corresponding imidazolium salt which was substituted with adamantyl groups to provide sufficient steric hindrance to protect the reactive carbene centre (Scheme 5).²⁶ It should also be noted that NHCs generally favour the singlet state.



Scheme 5: Synthesis of an *N*-heterocyclic carbene. The closed-shell singlet and the diradical (triplet) states are shown (R = alkyl, aryl, etc.).

The backbone of NHCs generally contain an electron-rich π -framework, which promotes electron donation into the carbon's out-of-plane p -orbital. Additional electronic stability is achieved from the σ -electron-withdrawal effects, caused by the electronegative nitrogen atoms, reducing the nucleophilicity of the carbene centre. This combination of π - and σ -effects increases the singlet-triplet gap, favouring the singlet state, by stabilizing the lone pair on the carbene centre.^{26,27,31} Triplet states tend to be highly reactive as they are biradicaloid systems. They can rapidly react with the solvent and excess reagents, whereas

in the singlet state the two electrons are paired. This same carbene has also been substituted with aryl groups, and although the steric hindrance was decreased, they were still isolable.²⁷ This study showed that the electronic effects are just as important as the sterics; when substituted with a *p*-tolyl substituent a π -effect was observed as the rings assumed a planar arrangement, causing conjugation with the carbene centre.²⁷

1.4 Main-Group Carbenoid Complexes

Since the first carbene was isolated in 1991 there has been an effort to isolate their main-group analogues, also known as carbenoids. The Group 14 carbene analogues have been studied extensively,^{32,33} and a considerable number of investigations have been performed for the Group 15 analogues.³³⁻³⁵ The discussion presented within this thesis will focus on the Group 13 analogues as there is still a lot to study in regards to their reactivity. Additionally, a neutral boron analogue has, to date, eluded detection both spectroscopically, and in condensed media.³² In 1998, carbene analogues containing Group 13 elements were still unknown; quantum chemical studies were performed to investigate the stability of these proposed compounds.³⁶ It was predicted that gallium-containing species would likely form stable compounds with sizeable singlet-triplet energy gaps.³⁶ The year after this study, the first Group 13 analogue of a carbene was reported as a gallium(I) complex containing a bulky diazabutadiene ligand (Figure 3, E = Ga).³⁷ This was achieved by preparing the corresponding gallium dichloride, which was subsequently reduced with potassium metal in the presence of 18-crown-6. As predicted,³⁷ this species contains a formally negative charge and was isolated in the solid state as its {K[18-crown-6](thf)₂} salt. This anion is a true analogue of a carbene, meaning that they are isoelectronic.

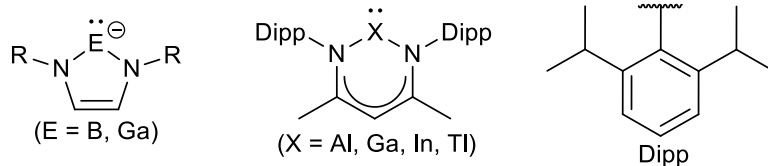
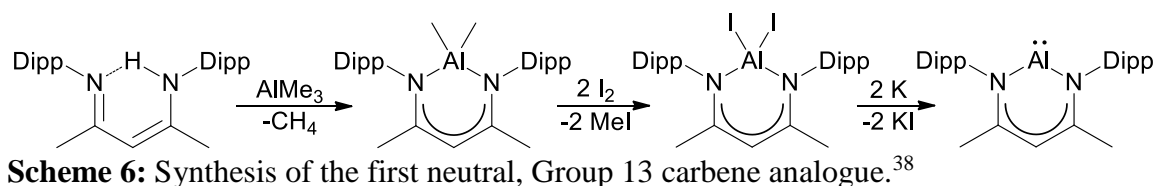


Figure 3: Group 13 carbene analogues isolated to date and the structure of the Dipp substituent (R = *t*-Bu or Dipp).

Synthetically, it would have been ideal if a neutral analogue of a carbene could have been isolated. Even though it would not be anionic, its reactivity should more closely resemble that of a dicoordinate carbene. For this to be achieved, research had to move away from the employment of the dianionic DAB ligand, and towards investigations of a monoanionic ligand. In the year 2000, the first monomeric aluminum(I) compound was prepared and this was also shown to be the first neutral, Group 13 carbene analogue ever isolated (Figure 3, X = Al).³⁸ In this study, the authors used the then recently reported,⁷ sterically crowded, bidentate β -diketiminate ligand (nacnac) to stabilize the reactive compound. First, the corresponding dimethylaluminum complex was formed by treating the ligand with trimethylaluminum, followed by the addition of two equivalents of iodine, I₂. Upon reduction with potassium the desired compound was obtained after three days (Scheme 6).³⁸ The solid state structure shows that the monomers are well separated without any close inter-molecular contacts between the aluminum centre and other atoms. The aluminum and ligand backbone form an essentially planar six-membered ring (Figure 4). This compound is analogous to a carbene as there is a nonbonded lone pair of electrons located on the aluminum centre and it is a neutral species.³⁸



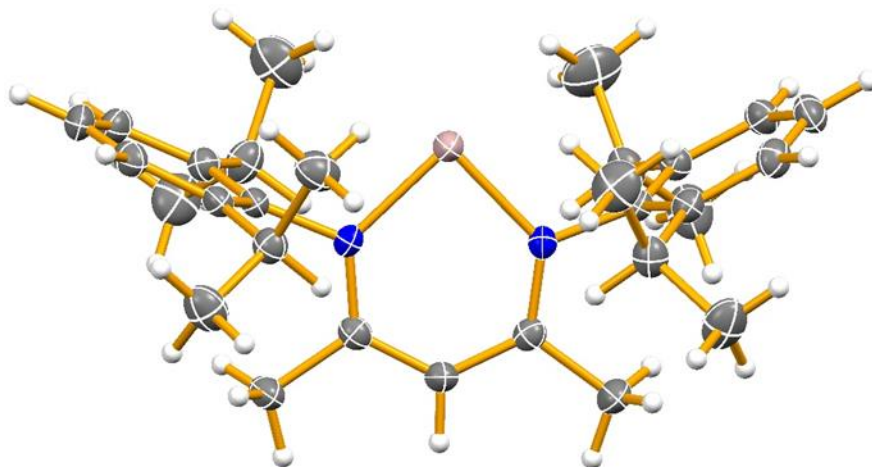


Figure 4: Solid state structure of the aluminum carbene analogue reported by Roesky *et al.*³⁸ Crystal structure obtained from the CSD (CCDC# 144530).³⁹ Thermal ellipsoids are drawn at the 50% probability level.

During the early 2000s, neutral carbene analogues of the remaining Group 13 elements, excluding boron, were reported; in 2000, Power reported the gallium analogue (Figure 3, X = Ga),⁴⁰ and Hill reported the indium analogue in 2004 (Figure 3, X = In).⁴¹ The first thallium analogue, with a modified diketiminate ligand, was isolated by Lappert in 2005,⁴² then Hill isolated a second, later that year, with the traditional ^{Dipp}nacnac group (Figure 3, X = Tl).⁴³ These three carbene analogues were prepared by first generating the Group 1 salt of the nacnac ligand, followed by the addition of the corresponding Group 13 halide (GaI, InI, or TlI).^{40,41,43} It should also be noted that the gallium analogue was prepared in the presence of potassium to reduce any I₂Ga(nacnac) that formed.⁴⁰ Similar to the aluminum analogue,³⁸ the six-membered heterocycles formed from gallium, indium, and thallium are also essentially planar.^{40,41,43} This is not the case for the first reported thallium analogue as it contains a trimethylsilyl group, bound to the chelating nitrogen atoms, instead of an aryl group.⁴² This causes the six-membered heterocycle to take on a boat conformation and is likely due to the lack of a rigid, “bowl-shaped” pocket, which aryl substituents would provide.

To date, all of the Group 13 elements have been isolated as neutral carbene analogues, except for boron. A computational study performed in 2006 showed that nacnac is not capable of stabilizing a singlet boron species; it was predicted to favour the triplet state by $14.50 \text{ kJ mol}^{-1}$,⁴⁴ however, no explanation of this preference was stated. The other Group 13 carbenoids have much higher singlet-triplet gaps, which likely contributed to their isolation while the boron analogue has eluded detection (Table 1). This same study also modeled three chemical reactions to investigate the reactivity of the Group 13 carbenoids.⁴⁴ A boron carbenoid of nacnac was shown to readily undergo C–H bond insertion and cycloaddition, in the presence of methane and ethene, respectively. The computations showed that there is no energy barrier for the dimerization of the boron analogue, as the reaction is thermodynamically favoured (Table 1).⁴⁴ Due to the boron analogue's predicted high reactivity, it would be surprising if nacnac was capable of stabilizing it in condensed media.

Table 1: Calculated singlet-triplet energy gaps and the relative energies for the dimerization process for the Group 13 carbenoids of nacnac at the B3LYP/LANL2DZ level of theory.

<i>Element (E)</i>	$\Delta E_{st} (\text{kJ mol}^{-1})^{44}$	$\Delta H_D (\text{kJ mol}^{-1})$	$\Delta G_D (\text{kJ mol}^{-1})$
B	-14.50	-295.47	-227.19
Al	191.33	1.85	62.26
Ga	227.86	14.41	76.65
In	230.41	11.30	73.72
Tl	226.27	3.76	44.22

Earlier in this section, it was stated that to prepare a true carbene (i.e. neutral) analogue, a monoanionic ligand would have to be utilized. Since it was predicted that this would likely be impossible,⁴⁴ Nozaki *et al.* reinvestigated the employment of DAB, with Dipp substituents, and they successfully isolated a boryllithium compound, isoelectronic with an NHC (Figure 3, E = B).⁴⁵ This was achieved by preparing the corresponding boron

bromide species, followed by its reduction with lithium naphthalenide. This compound could only be isolated in the solid state when dimethoxyethane (DME) was used as the reaction solvent. This resulted in a dimeric structure (Figure 5) that was thermally unstable above $-45\text{ }^{\circ}\text{C}$.⁴⁵ Due to the anionic nature of this compound, the B–Li bond length is $2.291(6)\text{ \AA}$.⁴⁵ Even though this compound contains bulky aryl substituents, which should prevent its dimerization, the long B–Li bond extends the dimerization environment outside of this “steric pocket”, with DME molecules linking the two monomer units.

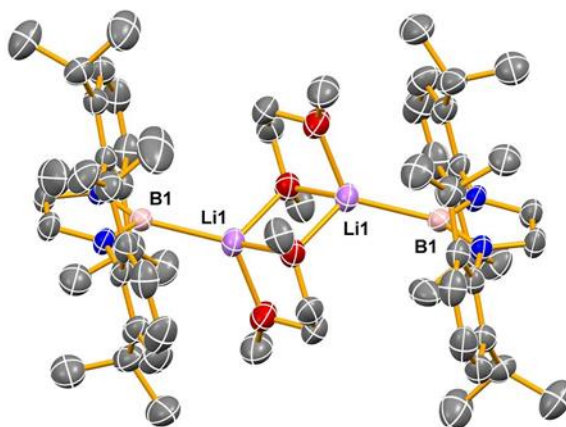


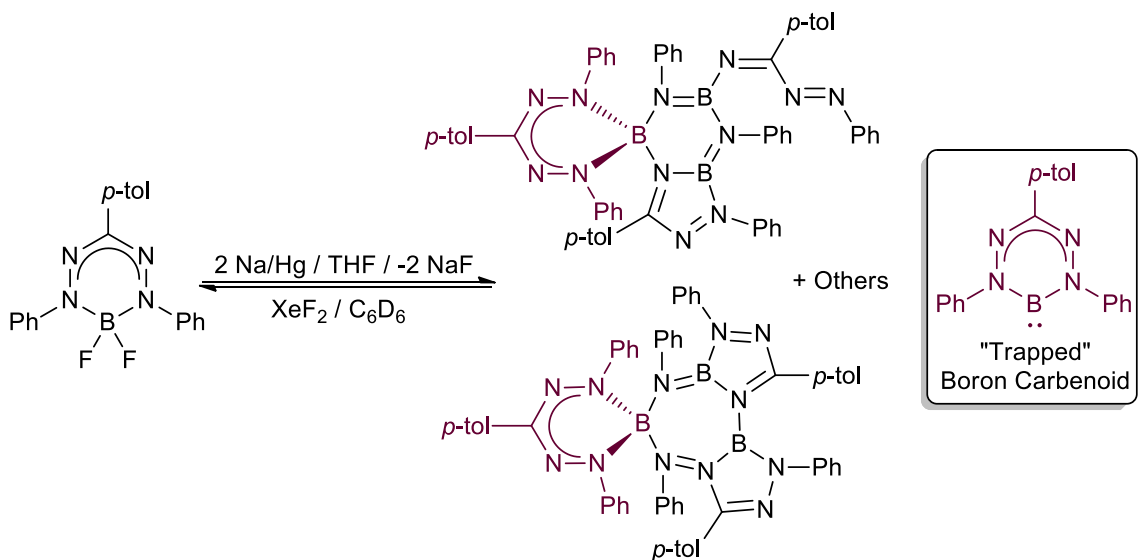
Figure 5: Crystal structure of the boryllithium–DME dimer reported by Nozaki *et al.*⁴⁵ Thermal ellipsoids are drawn at the 50% probability level. Hydrogen atoms have been omitted for clarity (CCDC# 604926).

If a neutral, singlet, boron carbenoid could be prepared, it should not contain ionic B–Li interactions that are present in the above. Another ligand which has been investigated for the stabilization of a neutral boron carbene analogue is the guanidinate ligand. It has been shown that this ligand is capable of stabilizing gallium and indium carbenoids,⁴⁶ and Cowley *et al.* have investigated its potential for the isolation of a boron analogue.⁴⁷ This study suggested that a combined DFT and MP2 approach should be used when studying this type of system, due to the overemphasis of triplet state stability in DFT calculations; this would result in the singlet-to-triplet energy gap (ΔE_{st}) being computed significantly

lower than the MP2 result. The MP2 approach may, more accurately, represent the energy gap that would be found experimentally, due to limitations with DFT. Cowley *et al.* also prepared two (guanidinate)boron dichlorides and the corresponding parent carbenoid was computationally modeled using DFT(B3LYP) and MP2 methods; ΔE_{st} of 25.10 and 42.26 kJ mol^{-1} were reported, respectively.⁴⁷ Although this predicted energy gap is much higher than the -26.06 (B3LYP) and 3.02 kJ mol^{-1} (MP2) calculated for the nacnac analogue,⁴⁸ attempts to reduce the (guanidinate)boron dichlorides were unsuccessful. Decomposition products were not reported and therefore, it is possible that this ligand *might* be capable of facilitating the isolation of a boron carbenoid, if alternative experimental methods were investigated.

To date, neutral boron analogues of a carbene remain elusive, likely due to their low singlet-triplet gaps and predicted high reactivities,⁴⁴ even evidence of them being generated *in situ* is rare. Instead of trying to overcome ΔE_{st} , trapping methods may be used to stabilize diradical (triplet) boron carbenoids, utilizing low-lying, ligand based, π^* orbitals.^{49,50} Very recently, a (formazanate)boron difluoride compound was prepared and treated with sodium amalgam, resulting in novel chemistry (Scheme 7).⁵⁰ A series of products were isolated, each of which were believed to incorporate a boron carbenoid fragment. An accompanying computational study suggested that a relatively stable boron diradical intermediate was being formed, and when two of the products, shown below, were treated with xenon difluoride, the (formazanate)boron difluoride was regenerated.⁵⁰ Even though the desired carbene analogue was not isolated, this is the first evidence that suggested that a neutral boron carbenoid *can* exist.⁵⁰ It was shown that boron diradical

species can be trapped, and can retain their carbenoid character even after being trapped, which could lead to “bottle-able,” boron based carbene reagents.

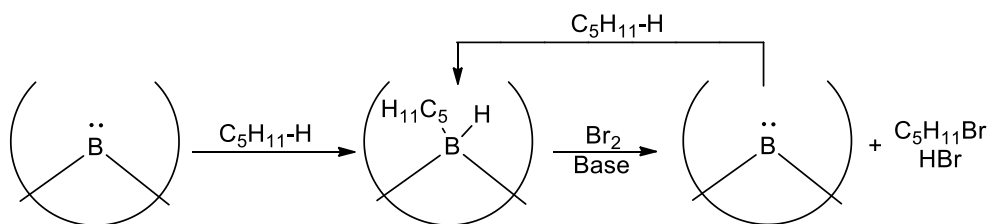


Scheme 7: Synthesis of the boron-containing products that incorporated a “trapped” boron carbenoid, reported by Chang and Otten.⁵⁰

1.5 The Importance and Implications of a Boron-Based Carbene Analogue

If a boron based carbenoid could be prepared, it should exist as an analogue to an NHC, and therefore might present similar reactivity. It has been shown that other Group 13 carbene analogues can be used *in lieu* of NHCs as ligands as they can also form adducts with metals centres.^{51,52} These heavier (Al, Ga, In, Tl) carbene analogues have also been used for the oxidative addition of C–F,⁵³ C–Br,⁵⁴ C–I,⁵⁴ C–O,⁵³ and C–In⁵⁵ bonds to the Group 13 elements. If isolated, the boron analogue should exhibit similar coordinating and oxidative properties. It has also been suggested that a low-valent boron-containing compound could be used for the efficient synthesis of haloalkanes from alkanes.⁵⁶ Currently, one of the only methods for this transformation (from general organic chemistry) is by radical halogenation, a reaction which offers poor control. This chemical transformation might be achieved by C–H bond activation, followed by cyclization, to

yield 1-bromopentane (Scheme 8).⁵⁶ Computations have already shown that a boron carbenoid can undergo C–H bond insertion.⁴⁴

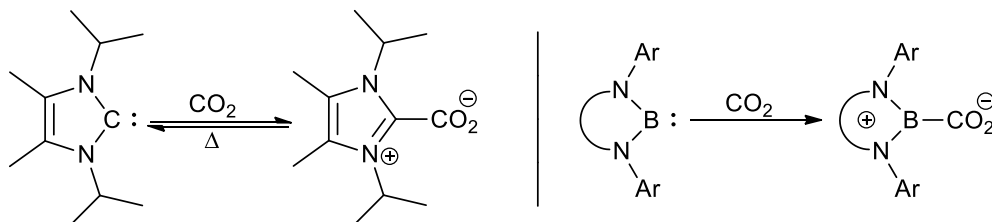


Scheme 8: Theoretical C–H bond activation of pentane *via* low-valent boron (the semi-circle represents the “bowl-shaped” pocket created by the aryl substituents).

Trivalent boron compounds are generally electrophilic, and therefore behave as Lewis acids, due to their empty *p*-orbital.⁵⁷ Boron reagents that exhibit nucleophilicity are rare and are persistent only at low temperatures. As previously mentioned, the boryllithium species is one of the only isolable nucleophilic boron reagents.⁴⁵ To accompany the isolation and characterization of this boron reagent, Nozaki *et al.* also studied its reactivity as a boryl anion. The boryllithium was treated with several electrophiles, such as benzaldehyde, chlorobutane or methyl triflate, resulting in the formation of borylbenzyl alcohol, butylborane or methylborane compounds, respectively.⁴⁵ This boryllithium compound could be used for the preparation of other synthetically important boron-containing molecules, however, it was thermally unstable above $-45\text{ }^{\circ}\text{C}$.⁴⁵ Due to this thermal instability, it is not synthetically convenient, and is not truly a “bottle-able” nucleophilic boron reagent. The preparation of other boron carbenoids should be investigated.

NHCs are reactive towards carbon dioxide, forming zwitterionic carboxylate compounds (Scheme 9).^{58,59} These carboxylate compounds can also decarboxylate, upon heating, to regenerate CO_2 and the carbene starting material,⁶⁰ as they have small bond dissociation energies.⁵⁹ The regenerative property of these adducts means that they can be

used as “catch and release” materials for CO₂ capture and storage.⁶⁰ Kuhn *et al.* prepared an NHC-carboxylate that reacted with thionyl chloride, forming a cationic NHC-acid chloride, which could be converted to the corresponding methyl ester.⁵⁸ A boron carbenoid should exhibit similar reactivity, and as previously mentioned, could be a valuable precursor for the synthesis of boron-containing compounds.



Scheme 9: The preparation of the first imidazol-2-carboxylate (left)⁵⁸ and the theorized boron carbenoid reactivity with CO₂ (right).

1.6 Aim of this Thesis

The heavy Group 13 (Al to Tl) carbene analogues have been isolated, characterized, and investigation into their reactivity has begun. A neutral boron analogue has eluded detection both in the solid state and *in situ*. It has been suggested that a boron based carbene analogue would have unique reactivity, which could lead to the preparation of synthetically valuable boron-based reagents, and which could also have application in catalysis. A new ligand will be designed, after computational optimization, for the stabilization of low-valent boron. The ligand itself will then be experimentally prepared, and its structural properties will be characterized. The reactivity, as well as the coordinating properties of this ligand will be investigated, and compared to the *industry benchmark*, 1,3-diketiminato, the nacnac ligand.

Chapter 2 – Results & Discussion

2.1 Computational Optimizations of a New Ligand Designed for the Stabilization of a Carbene Analogue of Boron

As previously stated, neutral boron carbenoids have never been isolated in the solid state, and their generation *in situ* has not been unequivocally proven. The lack of reported boron-based carbenes has been attributed to their low singlet-triplet energy gap, which is predicted to favour the triplet state, leading to high reactivities. If this functionality could be isolated, boron carbenoids could be invaluable reagents for inorganic and organic syntheses. To be isolated in the solid state, the carbenoid would likely have to be in a closed-shell singlet state, with the electron pair being located in an sp^2 orbital of boron. For this to be achieved, a new ligand would have to be designed, one capable of stabilizing a singlet state boron. As previously stated, a monoanionic ligand is preferred as this would lead to a neutral carbenoid. The previously discussed nacnac ligand was chosen as the starting point for this investigation. As can be seen in Figure 6, nacnac can be optimized in three symmetrically different locations, denoted here as R^1 , R^2 and R^3 .

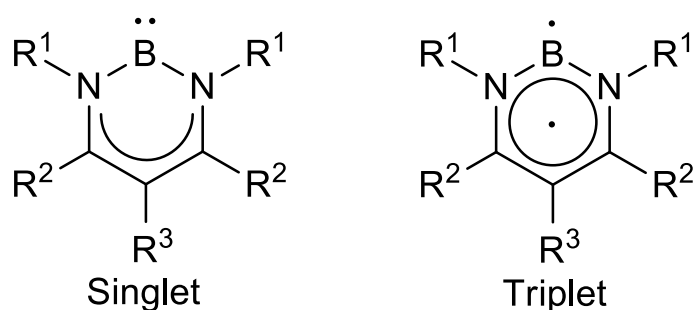


Figure 6: General structure of the boron carbenoid to be optimized. Both the singlet and triplet states are shown.

A computational study was performed, using DFT methods, to determine which substituents in each of the designated positions would give rise to the highest ΔE_{st} , and which would also favour the singlet state. While it was previously stated that DFT,

specifically the B3LYP hybrid-functional, over-emphasizes triplet state stability, for the purpose of this section this was determined to be unimportant. This is because the purpose of this portion of the study was not to quantify the singlet-triplet gap, but to observe the substituents that provided the largest singlet-triplet gap. After substituents had been chosen, for further investigations, a combined DFT and MP2 approach was employed. For computational efficiency, a hydrogen atom was used for the positions not currently being investigated. In the interest of time, the R³ position was not optimized within this thesis. The data presented in the followed tables was calculated at the B3LYP/6-31G* level of theory, using the Spartan '14 software package.⁶¹ ΔE_{st} was determined by separately optimizing both the singlet and triplet state carbenoids and calculating their energy difference (Equation 1); it should also be noted that a negative value implies that the triplet state is the ground state electronic structure.

$$\Delta E_{st} = E_{\text{Triplet}} - E_{\text{Singlet}} \quad (1)$$

The first position optimized was the one located on the chelating nitrogen atoms, denoted as R¹. The data are presented in Table 2. For this position, only sterically bulky groups, such as various aryl substituents, were chosen for investigation. This is because the steric protection afforded by the bulky groups should prevent dimerization of the carbenoid. It had previously been shown that electron donating groups increase the singlet state stability of carbenes,²⁷ and therefore one would have suspected that the mesityl (Mes) substituent should give the largest singlet-triplet gap. This was not the case, however, as it was shown that the *para*-tolyl substituent favours the singlet state by over 13 kJ mol⁻¹, compared to Mes. This has been attributed to the π -effect that Arduengo *et al.* reported for NHCs.²⁷ As can be seen in Figure 7, the aryl substituents assume an almost planar

arrangement with the six-membered heterocycle. This leads to conjugation between the aromatic rings and the out-of-plane p -orbital on boron, stabilizing the singlet state. This is not observed when R^1 is substituted with Mes, as the presence of substituents in the *ortho*-positions of the aryl groups, cause them to rotate out of the plane.

Table 2: Modifications of R^1 to obtain the largest singlet-triplet gap at the B3LYP/6-31G* level of theory ($R^2, R^3 = H$).

<i>Entry</i>	R^1	$\Delta E_{st} (kJ mol^{-1})$
1	Mes	-18.88
2	Dipp	-15.07
3	<i>t</i> -Bu	-6.90
4	Ph	-5.96
5	<i>p</i> -tol	-5.41

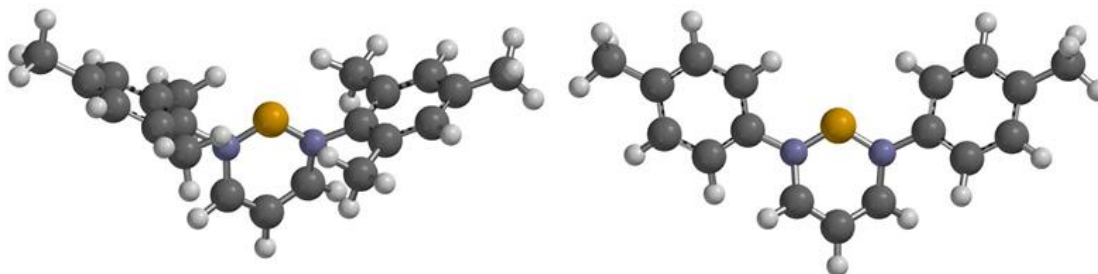


Figure 7: Graphical representations of the singlet states of Entry 1 (left) and Entry 5 (right) from Table 2.

After optimizing the R^1 position, the same method was used for the optimization of R^2 . Even though the R^1 position was already optimized, for computational efficiency, hydrogen atoms were used for both R^1 and R^3 . Since it had already been shown that the π -effect has a considerable effect on the stabilization of these systems, substituents that were known to be good π - and/or σ -donors were chosen for this investigation. To emphasize this donation effect, the trifluoromethyl (CF_3) substituent, a known electron-withdrawing group, was also investigated, and it was shown to greatly favour the triplet state. The dimethylamino substituent is generally considered to be more electron donating than ethoxy,⁶² however, the calculations presented in Table 3 suggest that the oxygen-based

substituents are more stabilizing. This may be because oxygen is more electronegative than nitrogen, as it has been shown that inductive effects stabilize carbenoid character by reducing the nucleophilicity. This same explanation was used to explain why CF_3 destabilized this system, however, ethoxy substituents contain π -electrons, and it is a *combination* of π -donation and σ -withdrawing effects that stabilize carbenes.²⁷ From this study, it was found that the ethoxy substituent provided the highest ΔE_{st} , and therefore it was chosen for further investigations.

Table 3: Modifications of R^2 to obtain the largest singlet-triplet gap at the B3LYP/6-31G* level of theory ($\text{R}^1, \text{R}^3 = \text{H}$).

<i>Entry</i>	<i>R²</i>	<i>ΔE_{st} (kJ mol⁻¹)</i>
1	CF_3	-34.15
2	Ph	-28.37
3	Me	-18.80
4	NMe_2	13.09
5	OMe	22.39
6	OEt	23.12

2.2 Computational Investigations of the Optimized Boron Carbenoid

After individually optimizing the designated substituent positions, a full computational study was performed on the optimized, theoretical compound ($\text{R}^1 = p\text{-tol}$, $\text{R}^2 = \text{OEt}$, $\text{R}^3 = \text{H}$). For simplicity, the optimized singlet state boron carbenoid will be referred to as **1s**, and the triplet state as **1t**. The computations showed that, for this ligand system, **1s** is the favoured ground-state electronic configuration, and it assumes C_1 point group symmetry (Figure 8). For computational efficiency, when calculating singlet systems, the electronics are restricted, and therefore a closed-shell singlet state always results. To ensure that the ground-state singlet was not open-shell (broken-symmetry), the singlet state calculations were repeated, unrestricting the SCF by allowing the α and β electrons to mix; the electronic configuration converged to **1s**. Computationally it was

found that this system has a ΔE_{st} of 13.98 kJ mol⁻¹ at the B3LYP/6-31G* level of theory; this is 40.04 kJ mol⁻¹ greater than that of the nacnac analogue.⁴⁸ As stated above, this compound was also studied by second-order Møller-Plesset methods and it was found to have a ΔE_{st} of 36.85 kJ mol⁻¹ at the MP2/6-31G* level of theory. For computational efficiency, the *p*-tolyl substituents were replaced with phenyl groups for the calculations performed at the MP2 level of theory.

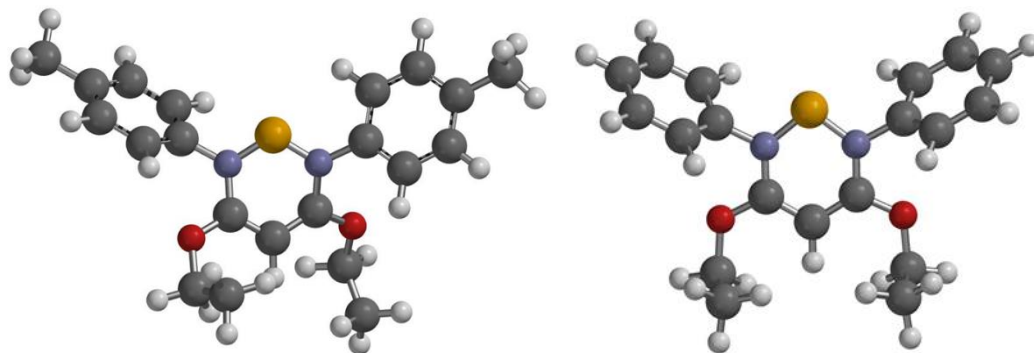


Figure 8: Graphical representations of **1s** at the B3LYP/6-31G* (left) and MP2/6-31G* (right) levels of theory.

The predicted electronic nature of **1s** is consistent with those reported for the Group 13 analogues of nacnac.⁶³ The lone-pair of electrons is located on boron, and occupies the HOMO of **1s**; the LUMO of this compound is also predominantly located on boron (Figure 9). Due to the locations of the HOMO and LUMO, this compound will likely exhibit both nucleophilic and electrophilic character at boron, which could potentially result in its dimerization. Since the bulky substituents were specifically chosen to prevent dimerization, the two molecules would have to align orthogonally to each other for this to occur. The dimer of this compound, **1d**, was optimized at the B3LYP/6-31G* level of theory (Figure A1) and its thermodynamics were also computed at the same level of theory. The enthalpy and Gibbs free energy of dimerization were determined according to Equations 2 and 3, respectively. Similar to the findings reported by Chen *et al.*,⁴⁴ it was

found that the dimerization of **1s** is thermodynamically favoured at room temperature ($\Delta H_D = -305.19 \text{ kJ mol}^{-1}$, $\Delta G_D = -229.05 \text{ kJ mol}^{-1}$). Although the computations show that it is thermodynamically favourable for **1s** to dimerize, experimentally, the presence of the aryl substituents should prevent self-oligomerization. The difference between the findings presented here, and those reported for nacnac, is that for the new boron carbenoid, the singlet state should be stable. It could potentially be synthesized, possibly as its dimer.

$$\Delta H_D = \Delta H_f \{ \text{dimer} \} - 2 \cdot \Delta H_f \{ \text{singlet carbenoid} \} \quad (2)$$

$$\Delta G_D = \Delta G \{ \text{dimer} \} - 2 \cdot \Delta G \{ \text{singlet carbenoid} \} \quad (3)$$

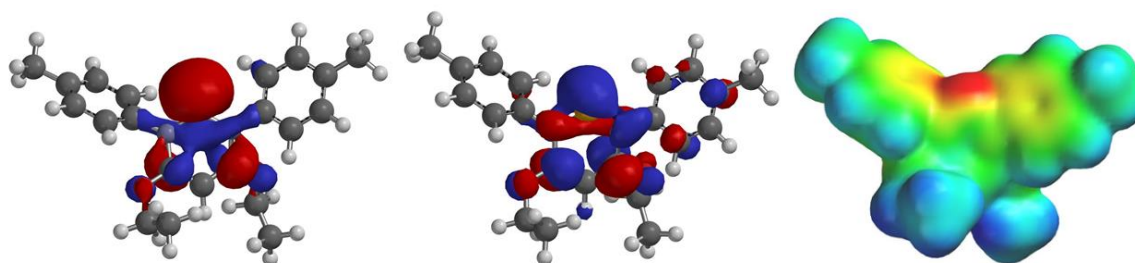
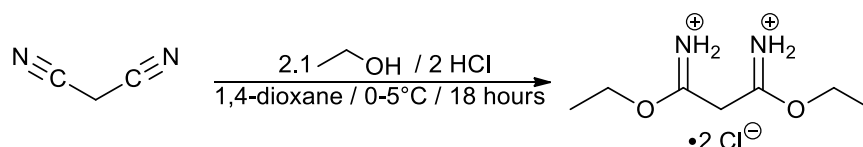


Figure 9: HOMO (left), LUMO (middle), and the electrostatic potential map (right) of **1s**. Calculations performed at B3LYP/6-31G* level of theory.

2.3 Experimental Ligand Preparation and Structural Investigations

Following the computational investigations, a retrosynthetic analysis was devised in an attempt to prepare **1s**. It was decided that a ligand would be prepared followed by its treatment with a boron-containing compound. The ligand, of the same general structure as that shown for **1s**, was synthesized by first preparing its neutral, precursor. One of the readily available starting materials, chosen for the synthesis of the ligand precursor, was diethyl malonimidate dihydrochloride (DEMHC1) (Scheme 9). This was a commercially available product, however, upon spectroscopic investigation it was found to contain a large amount of unidentified impurities. Literature preparations of this compound were thus investigated,⁶⁴ and it was found that the best method for preparing DEMHC1 does not

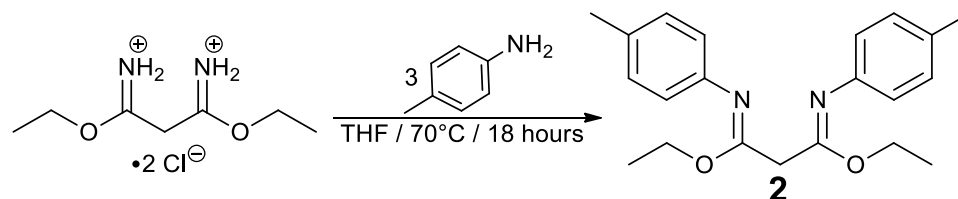
follow most of the principles of Green Chemistry.⁶⁵ This is because every synthesis involves the use of hydrogen chloride gas, and a substantial amount of solvent for a relatively small scale reaction (*ca.* 800 mL of solvent for 10 g of starting material).^{66,67} Since DEMHCl is used as a starting material for many BOX-type ligands,⁶⁸ a greener method was developed and is reported herein. Malononitrile was treated with excess ethanol in the presence of *anhydrous* hydrogen chloride (Scheme 10). Hydrogen chloride gas had previously been used, as it could be readily dried, and DEMHCl is susceptible to hydrolysis; the use of traditional *aqueous* HCl was not appropriate. To replace HCl gas, anhydrous HCl was added as a solution in 1,4-dioxane and the resulting suspension stirred overnight in an ice bath; DEMHCl was isolated in a 46 % yield. It was also found that adding an extra 30 mL of 1,4-dioxane, increased the yield to 86 %, which is comparable to that reported in the literature.^{66,67} Even though DEMHCl is insoluble in organic solvents, other than DMSO, this dilution likely reduced the likelihood of multiple ethanol additions to the electrophilic iminium, leading to an increased yield of the desired product. The total amount of solvent used for this reaction is only about 10 % of the amount that is used in current literature procedures.



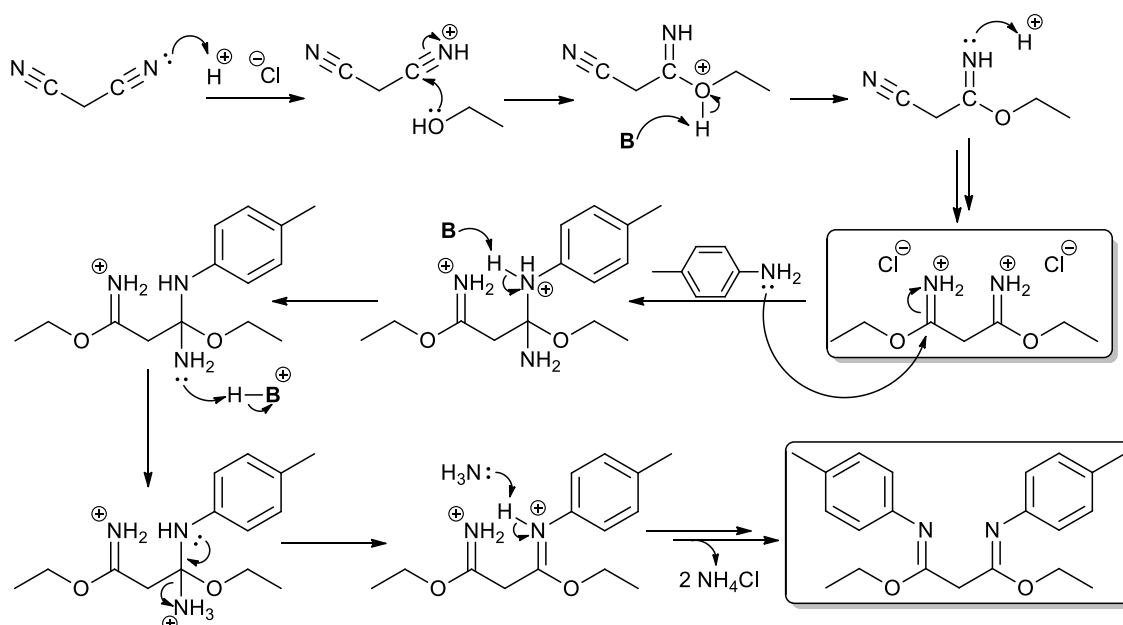
Scheme 10: Gaseous HCl-free synthesis of diethyl malonimidate dihydrochloride.

After preparing the starting material, the ligand precursor, diethyl-*N,N'*-bis(*p*-tolyl)malonimidate (**2**) was prepared by mixing DEMHCl and *p*-toluidine at a THF reflux (Scheme 11). The ligand precursor was isolated as a pale yellow oil, in a 30 % yield, after purification by column chromatography. For simplicity, this ligand precursor will be

referred to as NocNoc, and its corresponding anionic ligand as nocnoc. Although mechanistic studies were not performed on this reaction (Scheme 12), it is believed that the nitrogen atom in *p*-toluidine, undergoes nucleophilic addition to the electrophilic carbon of the imine followed by a deprotonation/protonation step resulting in the evolution of ammonia; there was also evidence of ammonium chloride in the NMR of the crude product.



Scheme 11: Synthesis of diethyl-*N,N'*-bis(*p*-tolyl)malonimidate, **2**, NocNoc.



Scheme 12: Proposed mechanism for the formation of DEMHCl and NocNoc (**B** = Brønsted base).

For most of this work, it was believed that NocNoc was a room temperature liquid, and therefore crystallization was not expected to occur. However, upon sitting at 5 °C for one week, clear, colourless, crystals were obtained. The X-ray structural analysis was consistent with the results from other spectroscopic techniques (Figure 10). It was also found that the aromatics exhibited π -stacking interactions (Figure A3). The melting point

of the crystals was determined to be slightly above room temperature, at 42 °C. It likely remained in the liquid state for so long due to strong interactions with trace amounts of a coordinating solvent.

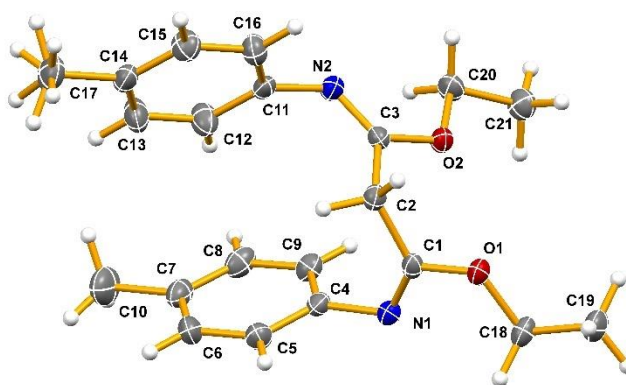
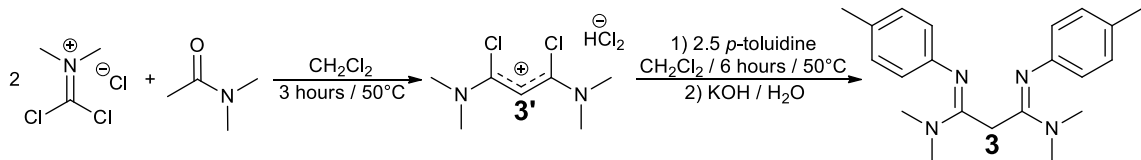


Figure 10: Solid state structure of NocNoc, **2**. Thermal ellipsoids are drawn at the 50% probability level.

Although it wasn't investigated computationally in any depth, the dimethylamino derivative was also prepared, to add to the toolbox of anionic *N,N'*-chelating ligands. Following a procedure similar to that reported by Lee,⁵⁶ Viehe's salt⁶⁹ was treated with dimethylacetamide, resulting in an intermediate, malonyl cyanine hydrogen dichloride (**3'**), which had previously been isolated and characterized (Scheme 13).⁵⁶ After the addition of *p*-toluidine and basic workup, 1,3-*bis*(dimethylamino)-*N,N'*-*bis*(*p*-tolyl)propanediimide (**3**) was isolated as an orange solid in a 55 % yield. Since this compound has the same structural backbone as Lee's ligand precursor,⁵⁶ **3** will be referred to as KnicNac, and its corresponding anionic ligand as knicnac, as originally termed by Lee. Orange, needle-shaped crystals of KnicNac were obtained, *via* the slow evaporation of a saturated diethyl ether solution (Figure 11). The ΔE_{st} of a boron carbenoid supported by knicnac was calculated to be 12.63 kJ mol⁻¹ at the B3LYP/6-31G* level of theory.



Scheme 13: Synthesis of 1,3-*bis*(dimethylamino)-*N,N'*-*bis*(*p*-tolyl)propanediimide, **3**, KnicNac.

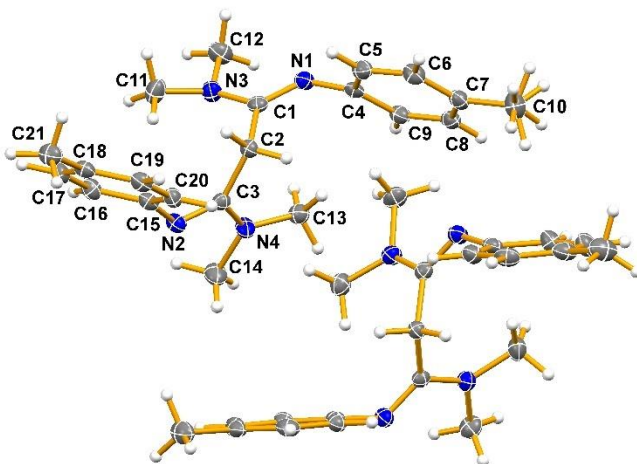
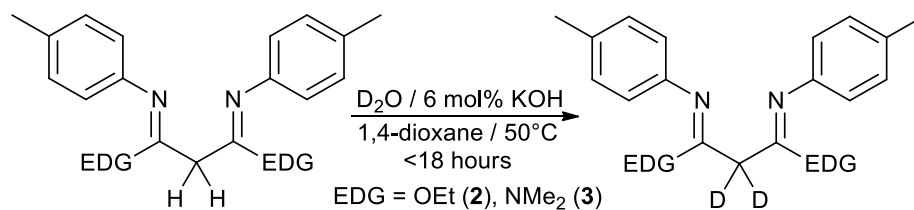


Figure 11: Solid state structure of KnicNac, **3**. There are two non-equivalent molecules in the unit cell. Thermal ellipsoids are drawn at the 50% probability level.

Both NocNoc and KnicNac are nitrogen-based analogues of a malonic ester. Due to this 1,3- substitution pattern, both **2** and **3** are predicted to have acidic α -protons. To show that these positions are, in fact, acidic, a deuterium exchange study was performed. Individually, each ligand precursor was dissolved in 3 mL of a 2:1 mixture of D_2O : 1,4-dioxane. These mixtures were stirred overnight, with mild heating, in the presence of a catalytic amount of hydroxide. It was concluded that both **2** and **3** underwent 100 % deuterium exchange at the α -position. In the 1H NMR, the singlets corresponding to the α -protons were no longer present, and the other chemical shifts were all experimentally identical, suggesting that it was not just a deprotonated species. The kinetics of this reaction were not studied; however, the fact that these ligands have acidic properties will be exploited in a later section.



Scheme 14: Determination of the relative acidity of the ligand precursors at the α -position *via* deuterium exchange.

If the R³ (α -) position of these ligands were to be functionalized, experimentally it would be achieved using a method similar to a malonic ester synthesis. Since deuterium exchange showed that this position is acidic, it would be deprotonated, followed by treatment with an electrophile, such as an alkyl halide. Since these ligands are predicted to coordinate as anionic ligands, they will first have to be deprotonated, resulting in the delocalization of the negative charge on the NCCCN backbone (Figure 12).

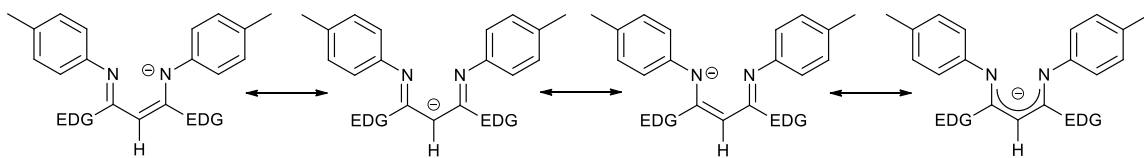
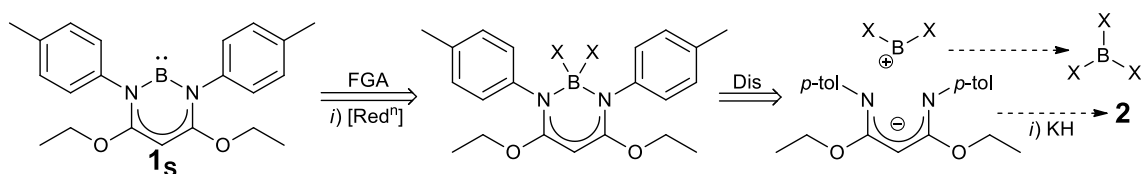


Figure 12: Resonance structures of the anionic N,N' -chelating ligands. The resonance hybrid is explicitly shown on the right.

2.4 Experimental Investigations of the Isolation of a Boron Carbenoid

After preparing the computationally modeled ligand, several synthetic methods were tried in attempts to isolate the elusive boron-based carbene analogue. The retrosynthetic analysis of **1s**, which was pursued in this study, is shown below (Scheme 15). It was believed that the best way to prepare this compound was by a method similar to that attempted by Cowley *et al.*⁴⁷ First the corresponding boron dihalide complex would be prepared, followed by the application of reductive methods. Attempted syntheses of the boron dihalide complexes were begun by first treating NocNoc with potassium hydride, which resulted in the evolution of gas (presumed to be H₂). The *in situ* potassium salt was then treated with a boron trihalide (BF₃, BCl₃ or BBr₃) in either ethereal or hydrocarbon

solvent. Unfortunately, there was no definitive spectroscopic evidence of such species actually being generated. No method could be found to isolate X-ray quality crystals, and NMR proved to be inconclusive, since no protons are associated with the boron centre, and there is boron-hydrogen coupling in the ^1H NMR. The ^{11}B NMR contained a new signal, that did not correspond to starting material or boric acid; while not a conclusive characterization, this was enough evidence to proceed forward in an attempt to isolate **1s**.



Scheme 15: Retrosynthetic analysis of the boron carbenoid, **1s** (X = F, Cl or Br).

After possibly preparing a series of boron dihalides, the purported products were treated with several reducing agents, which included potassium metal, lithium naphthalenide, and potassium-graphite (KC_8).⁷⁰ None of the tests with potassium resulted in any conclusive evidence for the desired reaction having occurred. Lithium naphthalenide is a stronger reducing agent than potassium, as lithium, in ethereal solvents, can be activated by a catalytic amount of naphthalene, and this aromatic radical is the active reducing agent. The reaction between the boron dibromide and lithium naphthalenide showed evidence of a REDOX reaction. Crystals were isolated from this reaction mixture, however, these were determined to be the previously reported $\text{LiBr}\cdot\text{DME}_2$.⁷¹ These crystals were present in a near stoichiometric amount (i.e. 2 molar equivalents) and, therefore, this suggests that the lithium had been oxidized, and therefore *something* had to have been reduced. In addition, the two bromide anions had to have been abstracted from *somewhere*. Combined, this is good evidence to support the idea that, at some point, the boron

carbenoid, either singlet or triplet, may have been present in solution. However, no evidence of it, or any degradation products, was obtained.

Another interesting finding came from the boron dichloride reaction. When treated in THF with two equivalents of potassium-graphite, followed by filtration, a dark yellow, slightly opaque, solution resulted. Again, characterization was inconclusive, and therefore it was decided that the reactivity would be studied in an attempt to “trap” the carbenoid. Following standard Schlenk techniques,⁷² the solution was opened to a flow of CO₂, and the solution immediately turned clear and colourless. To reduce the likelihood that this observation did not arise from a reaction with residual water, the CO₂ was passed through two drying tubes prior to it entering the reaction vessel. Again, spectroscopic evidence did not yield any significant insight into the observed reactivity. However, it is possible that the corresponding boron carboxylate, shown in Scheme 9, was prepared. From the findings presented herein, there is no experimental or spectroscopic evidence supporting the preparation of a boron-based carbenoid. However, these observations, combined with the accompanying computational study, do suggest that this ligand system should be further investigated. It is still possible that a neutral boron carbene analogue could be isolated.

2.5 Experimental Determination of the Electronic Donating Abilities of nocnoc and knicnac: The Preparation and Structural Investigation of Rhodium Carbonyl Complexes

Unfortunately, a boron carbenoid was not successfully prepared in the present study; however, the reactivity and coordination of the ligands were further investigated. Both nocnoc and knicnac have substitution patterns similar to those of BOX ligands, and therefore could prove to be useful on the frontier of organometallic research. The first step

in this process was to determine the electronic donating properties of the ligands. One method often used to determine this property is to prepare, and study, metal carbonyl complexes that incorporate the ligand of study. This is based on the concept known as π -backbonding, in which filled d -orbitals of the metal donate electron density into empty π^* -orbitals on the carbonyl ligand (Figure 13). The addition of electron donor ligands to metal carbonyl compounds increases the electron density of the d -orbitals and therefore, also increases the d - π^* backbonding into the carbonyl. This effectively reduces the C–O bond order, which can be studied spectroscopically to compare the effects of the donor ligands.

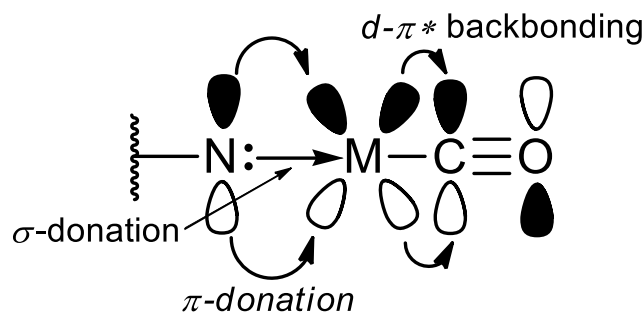
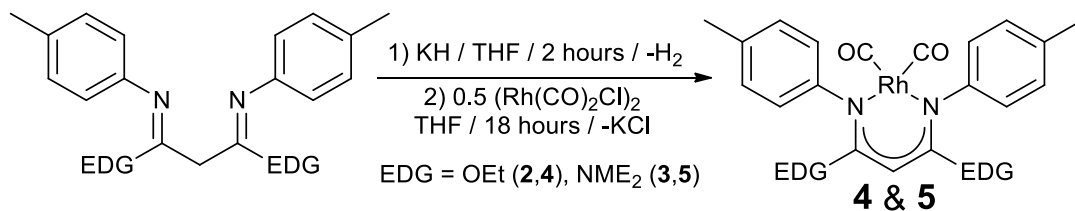


Figure 13: d - π^* backbonding in a metal carbonyl compound containing a nitrogen donor ligand (M = metal centre).

For this study, rhodium was chosen as the metal centre to study. Rhodium(I) is not paramagnetic, and therefore can be studied by NMR. Also, the rhodium(I) dicarbonyl of nacnac had previously been prepared,⁷³ and studied,⁷⁴ and therefore was available for direct comparison to the similar N,N' -chelating ligands reported herein. The rhodium dicarbonyl compounds of nocnoc (**4**) and knicnac (**5**) were prepared under the same set of conditions, as illustrated in **Scheme 16**. First, their corresponding potassium salts were generated *in situ*, by treatment of the ligand precursor with potassium hydride, followed by the dropwise addition of a chlorodicarbonylrhodium(I) dimer solution. Upon purification and

crystallization, compounds **4** and **5** were isolated as orange/yellow, cubic crystals (Figure 14).



Scheme 16: Synthetic route to the rhodium dicarbonyl compounds, **4** and **5**.

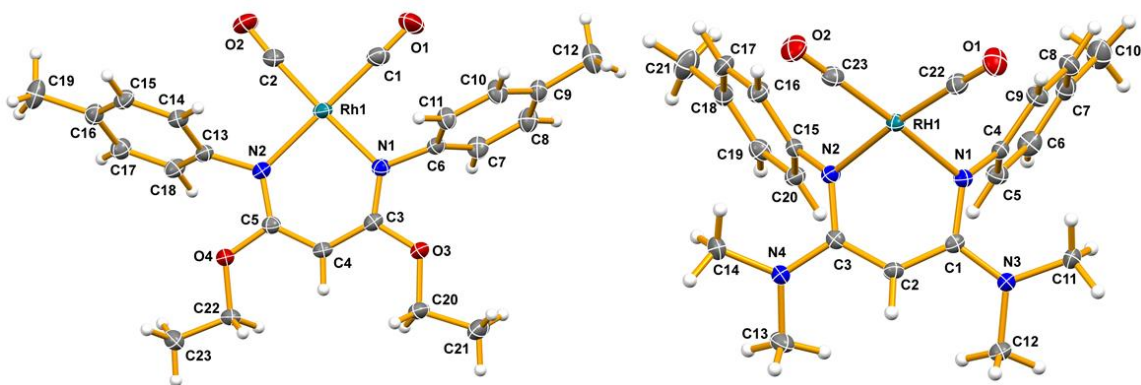


Figure 14: Solid state structures of the rhodium dicarbonyl compounds **4** (left) and **5** (right). Thermal Ellipsoids are drawn at the 50% probability level.

The solid state structures present some insights into the structural and bonding features of these ligands. As predicted, the aryl groups rotate out of the plane, forming a “bowl-shaped” pocket around the rhodium centre, in **4**. The ethoxy groups of nocnoc also behave as would be expected, pointing away from the aryl substituents to reduce steric interactions. Finally, the six-membered heterocycle present in **4** is essentially planar. The structure of **5**, on the other hand, is far from what was expected *a priori*. The C₂ carbon atom, as well as the rhodium atom, pucker out of the plane,⁷⁵ resulting in the six-membered ring assuming a boat-type conformation (Figure 15). Also observed in the structure of **5** is that the dimethylamino substituents are almost co-planar with the six-membered ring, suggesting *sp*² hybridization of the dimethylamino nitrogen atoms. This would result from an increase in bond-order of the C–N bonds, indicating a high degree of electron donation

into the six-membered ring. Additionally, the co-planarity of these dimethylamino substituents sterically clash with the *p*-tolyl groups, causing them to rotate further backwards than anticipated. This “steric clash” likely explains the observed ring puckering.

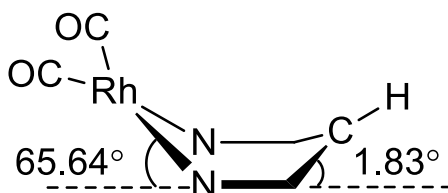
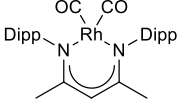
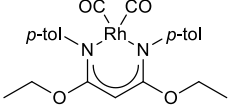
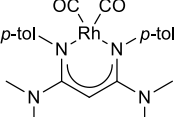


Figure 15: Graphical representation of the “puckering” observed in **5**. Some substituents have been omitted for clarity.

After preparing the rhodium carbonyl compounds, three quantitative methods were chosen to investigate the carbonyl groups.¹ The first was to measure the carbonyl symmetric and asymmetric stretching frequencies in the infrared (IR) spectra. Ligands that have greater donor properties will shift both frequencies to a lower wavenumber. The second method is to measure the C–O bond lengths obtained from the solid state structure. Finally, the carbonyl chemical shift in the ¹³C NMR spectra can be observed. However, this is not usually an accurate method of quantification as the chemical shift is quite fluxional depending on the chemical environment and can mask information about the carbonyl.¹ The observed results, from all of these three methods, arise from the reduction of the C–O bond-order.

The IR spectra of all three compounds were obtained as KBr pellets, and the ¹³C{¹H} NMR data was collected in C₆D₆. The IR stretching frequencies, as well as the C–O bond lengths were also computed at the B3LYP/LAN2DZ level of theory, using the solid state structures for the starting geometries. The data obtained from the experimental and computational studies for the two structures reported above, **4** and **5**, as well as the structurally similar (nacnac)Rh(CO)₂, are summarized in Table 4.

Table 4: Experimentally determined, and calculated, spectroscopic values corresponding to the carbonyl groups.

<i>Structure</i>	<i>Experimental</i> [†]			<i>Calculated</i>	
	ν_{CO} (cm^{-1})	C–O (\AA)	δ_{CO} (ppm)	ν_{CO} (cm^{-1})	C–O (\AA)
	2055, 1988	1.142(3), 1.142(3)	184.9	2016, 1959	1.171, 1.171
	2056, 1988	1.142(2), 1.137(2)	185.1	2025, 1962	1.170, 1.170
	2049, 1977	1.143(2), 1.142(2)	187.2	2016, 1951	1.172, 1.172

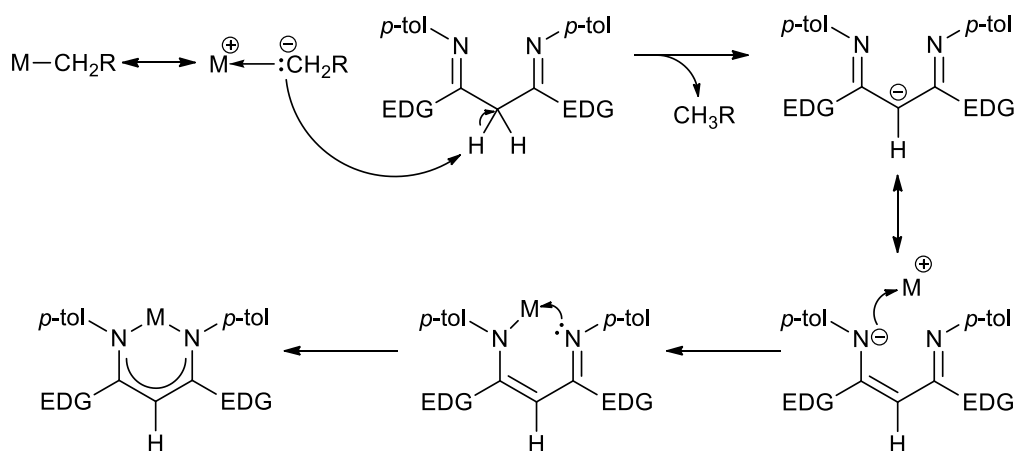
[†] Experimental data for (nacnac)Rh(CO)₂ was reported by Masuda *et al.*⁷⁴

It was found that nocnoc exhibits similar electronic properties to nacnac and that the knicnac ligand is a better donor than both nacnac and nocnoc. Computational results suggest nacnac is a better donor than nocnoc, however, experimentally they were found to be identical. Prior to this investigation, it was predicted that nocnoc would be a better donor than nacnac due to the presence of the electron donating ethoxy substituents. While nocnoc may be a better π -donor, the mesomeric electron-withdrawing effect of oxygen likely reduces its σ -donor properties. Therefore, it is believed that the increased π -effect is negated by the σ -withdrawing effect of nocnoc. Dimethylamino and the ethoxy substituents have similar donating effects, and therefore, knicnac should have similar a π -donating ability relative to nocnoc. As can be seen in Table 4, knicnac is overall a better donor than nocnoc. This can be explained by the facts that dimethylamino is a slightly better donor compared to ethoxy, and, the mesomeric electron-withdrawing effect is not as strong for the less electronegative nitrogen atom. It has been shown, by both experimental and computational methods, that nocnoc has similar donor abilities to nacnac, and that, knicnac

may be a better donor ligand than both nacnac and nocnoc. However, since **5** is structurally different from **4** and (nacnac)Rh(CO)₂ direct comparisons cannot be made.

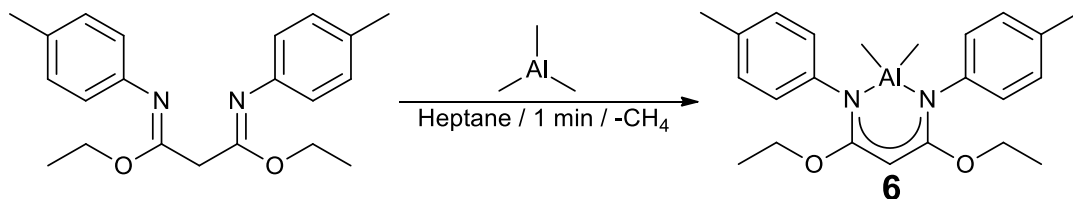
2.6 Structural Investigation into the Reactions of NocNoc with Low-Coordinate Organometallic Reagents

To further study the reactivity of nocnoc, **2** was treated with a variety of low-coordinate organometallic reagents. The low-coordinate organometallics chosen for this study are also Lewis acids. For this reason, the neutral ligand precursor, NocNoc, could be treated directly with the organometallic reagent, without first having to generate the anionic ligand. This is because the “carbanion” ligands of the organometallic are capable of deprotonating the α -protons of **2** (Scheme 17). This results in the generation of a thermodynamically stable, small molecule. For the reagents investigated within, this small molecule was a hydrocarbon gas. Computationally, in the gas-phase, it was found that the imine tautomers of NocNoc and KnicNac are favoured over the enamine by 15.49 and 34.89 kJ mol⁻¹ respectively, at the B3LYP/6-31G* level of theory. Therefore, their reactions with Lewis acids likely proceed as outlined in Scheme 15.



Scheme 17: Resonance structure of the Lewis acid explicitly showing its carbanion. This is utilized for the deprotonation of the ligand precursor’s α -protons, resulting in the evolution of a small molecule, and the formation of the corresponding metal complex (M = metal centre, R = short-chained alkyl).

The first organometallic reagent studied was trimethylaluminum (AlMe_3). A solution of AlMe_3 in hexanes was slowly added to a solution of **2** (Scheme 18). This resulted in the immediate evolution of gas, as well as the formation of a white precipitate. This gas was later confirmed to be methane from an NMR scale experiment which showed a new singlet at 0.16 ppm, in C_6D_6 , characteristic of methane.⁷⁶ Further investigations, *via* real-time analysis with a ReactIR spectrometer, found that the reaction was complete in less than one minute; indicative of an acid-base reaction. After recrystallization from THF, the solid state structure of **6** was obtained (Figure 16). From the solid state structure, it can be seen that the coordination of nocnoc is consistent with what is observed in **4**. When X-ray crystallographic data was collected at room temperature (298 K), the structure proved to be slightly different than that observed at low temperature (125 K) as emphasized in Figure 16. The ethoxy substituent in the structure obtained at 125 K has rotated out of the plane, and the low temperatures effectively “locked” this substituent in the observed position. However, at room temperature, a sufficient amount of thermal energy has been added for **6** to have undergone a phase change, causing the same substituent to rotate back into the plane of the six-membered ring. The thermal ellipsoids are larger for the room temperature structure due to the increased thermal motion at higher temperatures. It should also be noted that, surprisingly, this compound is air and moisture stable; crystals have been found unchanged after eight months of exposure to ambient conditions.



Scheme 18: Synthesis of the dimethylaluminum complex of nocnoc, **6**.

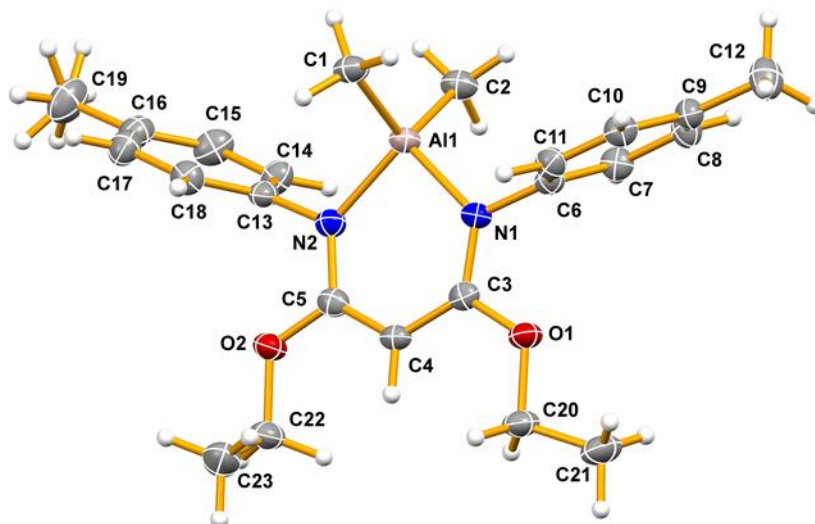


Figure 16: Solid state structure of the dimethylaluminum complex of nocnoc, **6**, at 125 K. Thermal ellipsoids are drawn at the 50% probability level.

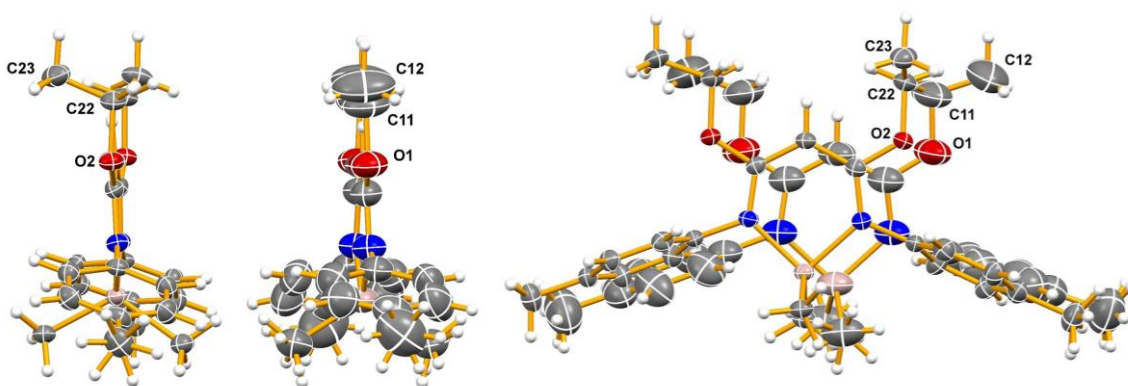


Figure 17: Solid state structures of **6** at 125 K (left) and 298 K (middle), as well as an overlay of both structures (right).

To further investigate the thermal behaviour of **6**, it was studied by differential scanning calorimetry (DSC). The DSC curve of **6**, Figure 18, collected with a heating rate of $10\text{ }^{\circ}\text{C min}^{-1}$, offers some evidence to support the phase change, the results of which are shown in Figure 17. There was an observed endothermic transition with an onset temperature of $-72\text{ }^{\circ}\text{C}$. The enthalpy, ΔH , associated with this transition is 0.55 kJ mol^{-1} . An exothermic transition was also observed at $-20\text{ }^{\circ}\text{C}$; $\Delta H = 0.97\text{ kJ mol}^{-1}$. While these values are quite low, they can clearly be seen on the DSC curve. The transition that appears between 0 and $20\text{ }^{\circ}\text{C}$ likely results from the loss of residual water, and the region between

45 and 145 °C is characteristic of oil impurities;⁷⁷ a pale orange oil impurity did coat the crystal sample. The sample was heated slightly above its onset melting temperature of 152 °C, to 170 °C, and was then cooled to -80 °C at a rate of 10 °C min⁻¹. The exothermic transition at 130 °C (freezing) was determined to be 0.85 kJ mol⁻¹ lower than the endothermic transition (melting), possibly due to the oil impurity being incorporated into the sample upon recrystallization. This recrystallized material was likely amorphous, because it crystallized rapidly, whereas the original sample of **6** had been crystallized by slow evaporation. Upon reheating the sample, the solid-solid transitions were not observed, additional evidence that the recrystallized material was less ordered, and therefore did not revert to the original morphology.

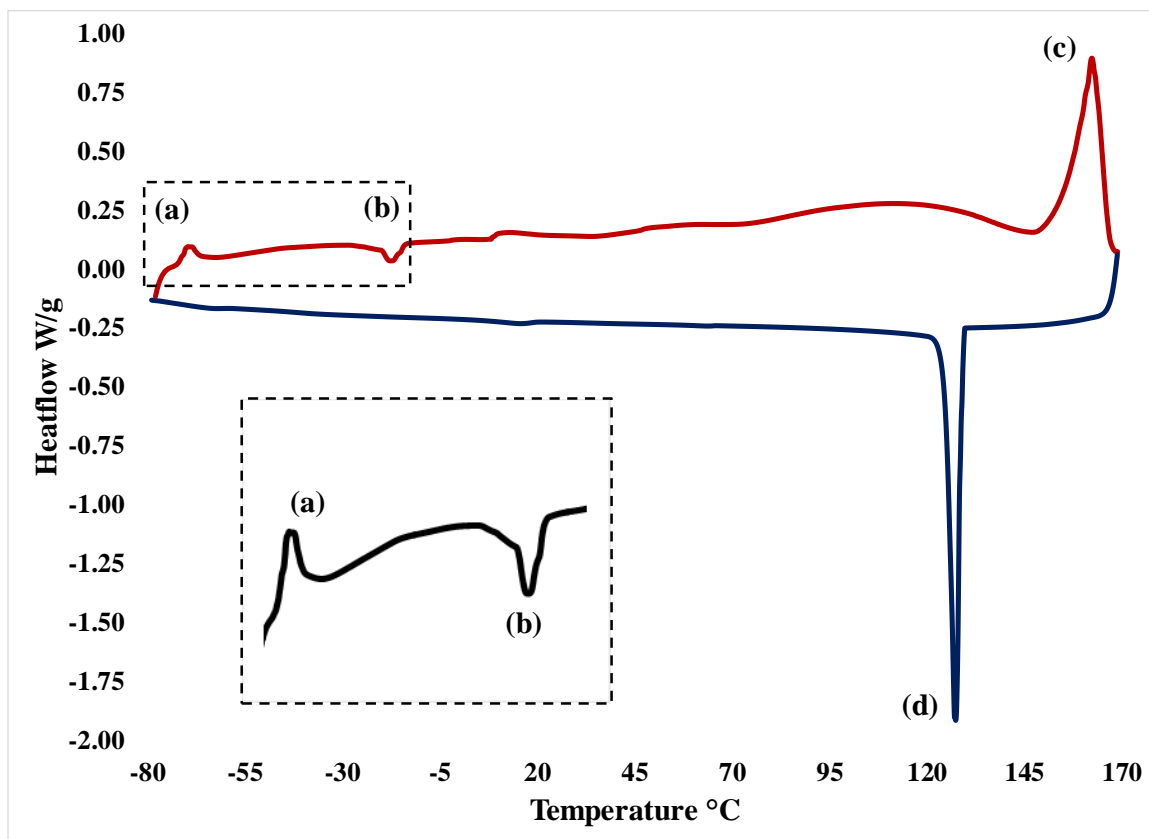


Figure 18: DSC curve of **6** collected with a heating/cooling rate of 10 °C min⁻¹. Positive heatflow indicates endothermic transitions. (a) solid-solid transition, (b) solid-solid transition, (c) melting point, (d) freezing point. The heating curve is shown in red and the cooling curve in blue.

The DSC curve showed two solid-solid transitions, and there could be more, but, the range between -148 and -80 °C was not probed. It would be expected that a third morphology would be observed if an X-ray analysis was performed on **6** between -72 and -20 °C. However, when data collection of **6** was performed at -50 °C the unit cell matched the room temperature structure. X-ray data of **6** was also collected at -100 °C and the unit cell was found match the 125 K structure. From this evidence it can be concluded that the observed phase transition likely happens at -72 °C as an endothermic transition; it would be expected that this transition would require energy. The nature of the exothermic transition at -20 °C remains a mystery, however, this does not result in a crystallographically observable transition; powder diffraction may give insight into this transition.

During the standard characterization of **6**, it was discovered that the methyl groups on the aluminum centre are highly shielded; they have a chemical shift of -0.25 ppm in the ¹H NMR, when run in C₆D₆. To further investigate this compound, the dipole was calculated from its optimized structure; geometry optimizations were performed at the B3LYP/6-31G* level of theory, using the crystallographic results for the initial geometries. It was found that **6** is a highly polar molecule with a dipole of 5.98 Debye. The dipole points from the C4 atom, through the Al atom (Figure A2). For comparison, water has a dipole of 2.09 Debye, when calculated at the same level of theory. The packing in this molecule's unit cell shows short contacts show that there are π -type interactions, causing **6** to pack with a modified herringbone motif (Figure 19). The crystalline material of this product was isolated as a *single*, large, crystal, with an approximate dimension of 15 x 5 x

2 mm³, for only 180 mg of material (Figure A4). This vast crystal network is most likely due to the strong intermolecular interactions found within its solid state structure.

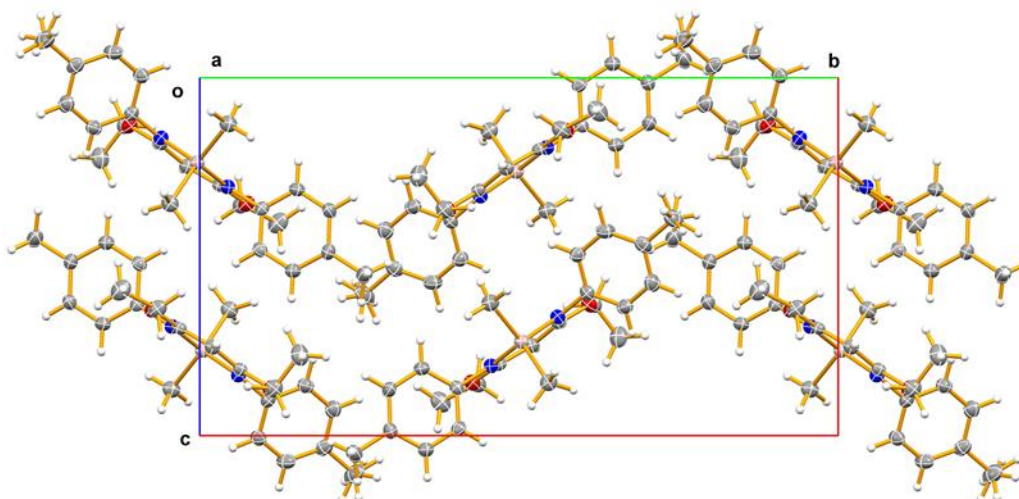
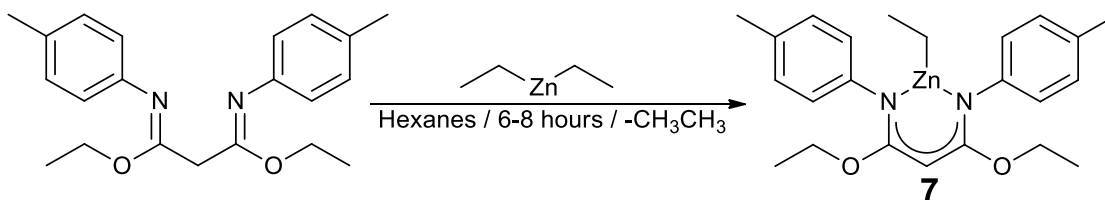


Figure 19: Solid state packing of **6**, viewed down the *X*-axis, showing the modified herringbone motif.

Another low-coordinate organometallic reagent investigated was diethylzinc (Et₂Zn). A solution of Et₂Zn in hexanes was slowly added to a solution of NocNoc, but no immediate change was observed (Scheme 19). This solution was not stirred, and the solvent was removed by slow evaporation resulting in large, block-like crystals of **7** (Figure 20). The small molecule (gas) evolved was confirmed to be ethane by NMR analysis; a new singlet was observed at 0.80 ppm, in C₆D₆, in the ¹H NMR.⁷⁶ Upon further experimentation, stirring this solution did not yield **7**. There is NMR evidence suggesting that this resulted in the formation of Zn(nocnoc)₂, however it has not successfully been isolated in the solid state. This observed reactivity could be a simple kinetic *vs* thermodynamic control situation; however, the *bis* complex was not investigated further. The elemental analysis (EA) of this compound was collected three times, and in each run the carbon-count was low. When recalculated, accounting for the loss of ethane gas from the complex, the previously obtained EA's were all within accepted experimental error for all three elements

(C, H, & N). This proposed decomposition is supported by the observation that a gas was evolved during the melting point acquisition. To date, the decomposition products have not been studied. Similar to **6**, this compound also appears to be air stable for at least two weeks.



Scheme 19: Synthesis of the ethylzinc complex of nocnoc, **7**.

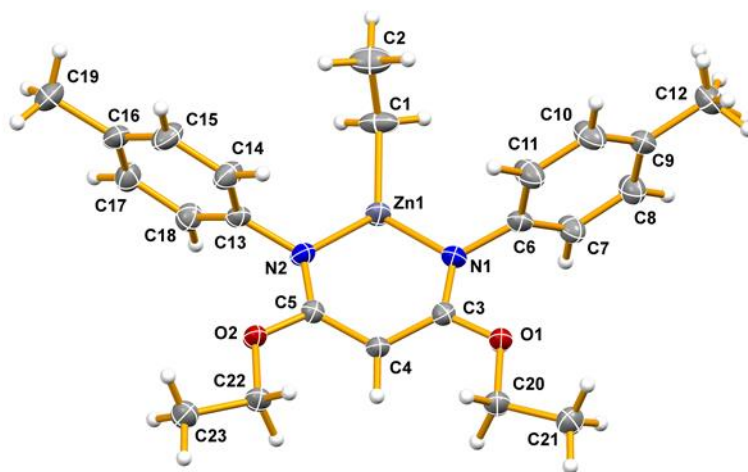


Figure 20: Solid state structure of the ethylzinc complex of nocnoc, **7**. Thermal ellipsoids are drawn at the 50% probability level.

Upon investigation of the structure of **7**, it was found that this ethylzinc complex dimerizes in a *face-to face* conformation in the solid state. X-ray crystallographic analyses of **7** shows that there are close contacts (2.594(2) Å) between the C4 and Zn atoms of separate monomer units (Figure 21 & Figure A5). These atoms *slightly* “pucker” from planarity; however, it is not as extensive as that shown in Figure 15 for the Rh carbonyl compound of **5**. To probe the nature of the Zn⋯C interaction between the monomer units of **7**, a QTAIM^{78,79} analysis was performed at the B3LYP/6-31G* level of theory. It has

been well established that the electron density and the Laplacian of the electron density at the bond critical point (BCP) correlate well with bond character.^{78,79} Covalent bonds generally display electron density values greater than 0.20 au with negative Laplacian values, and closed-shell interactions generally exhibit electron density values less than 0.10 au and positive values for the Laplacian. The electron density and Laplacian values for the BCP corresponding to the Zn···C4 interaction in **7** are 0.035 au and 0.109 au, respectively. This clearly suggests the presence of a weak closed-shell interaction with little to no electron sharing, one which is primarily electrostatic in nature. In addition, the calculated number of electrons shared between Zn and C4 is 0.203, which indicates a low bond order. A similar Zn···C interaction has been reported in a zinc-alkyne dimer, with electron density and Laplacian values of 0.037 and 0.095 au, respectively.⁸⁰ The values for the zinc-alkyne dimer, and those of **7** are surprisingly similar, suggesting the π -system of **7** is very electron-rich. Although this interaction has a low bond order, it is still an important interaction in the structure since two of them are sufficient to hold the dimer together in the solid state. Another diketiminate zinc dimer has been reported,⁸¹ however, to the author's knowledge, this is the first computationally investigated interaction of this type for an *N,N'*-chelating system.

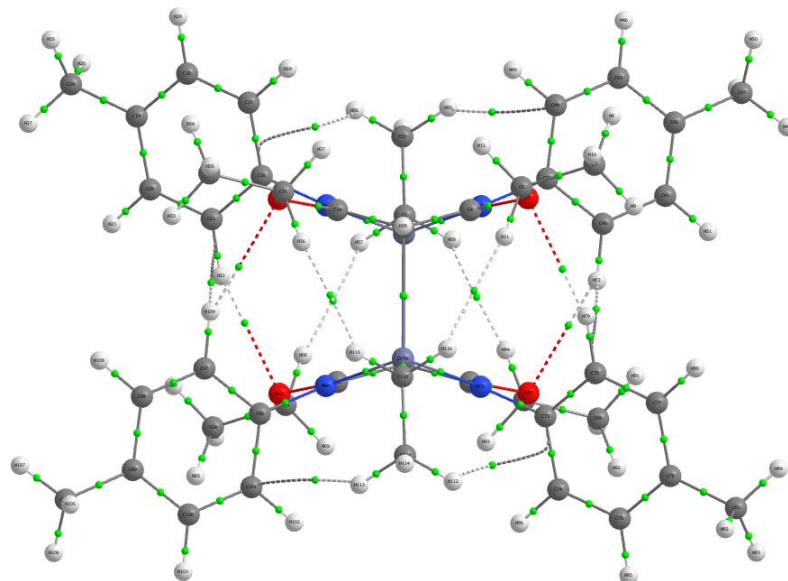


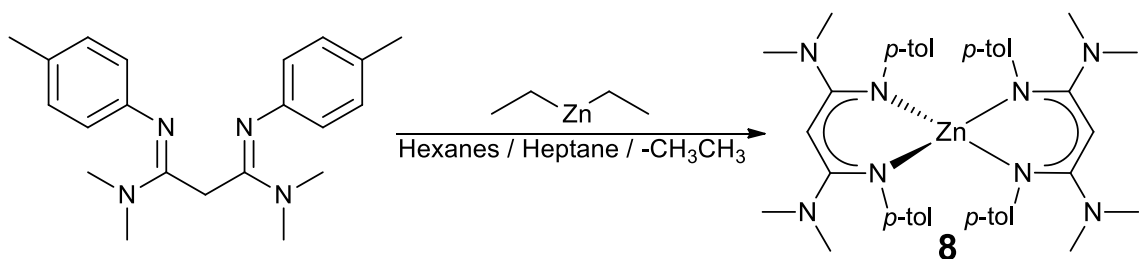
Figure 21: Bond critical points in the dimeric structure of **7** calculated at the B3LYP/6-31G* level of theory. The image was generated with AIMAll,⁸² and the BCPs are shown in green.

Another Lewis acid chosen for investigation was methylmagnesium bromide (MeMgBr). Initially, it was thought that this would react in a similar fashion to what is shown in Scheme 17. Upon the addition of MeMgBr to a THF solution of NocNoc, gas was immediately evolved. This was assumed to be methane, however, it was not spectroscopically confirmed. Small, clear, crystals of material were isolated, and both NMR and X-ray analyses suggested it was magnesium bromide, solvated with THF ($\text{Br}_2\text{Mg}\cdot\text{THF}_x$). To date, the $\text{BrMg}(\text{nocnoc})$ compound has not been successfully isolated, however, further investigations should be conducted employing non-coordinating solvents. This would be to ensure that the solvent does not displace the desired ligands of interest.

2.7 Structural Investigation into the Reactions of KnicNac with Low-Coordinate Organometallic Reagents

Since knicnac had previously been reported by Lee, its reactivity was not investigated in as great a depth as that of nocnoc was. Additional reactivity of knicnac can

be found in the thesis entitled: *Synthesis, Functionalization, and Coordination of Bulky *m*-Terphenyls and β -Diketiminates*.⁵⁶ Since interesting interactions were observed in the zinc complex, **7**, attempts to prepare its knicnac analogue were investigated. Due to time constraints, the ethylzinc complex of knicnac has not been successfully isolated. However, upon the addition of diethylzinc to KnicNac, crystals of a *bis*(knicnac) zinc complex, **8**, were isolated after it sat at -15 °C for one week (Scheme 20 & Figure 22). To date, this structure has not been fully interpreted. Interestingly, the complexed zinc is tetracoordinate, incorporating two equivalents of knicnac. The *p*-tol^{yl}knacnac analogue has been previously reported,⁸³ and it is structurally similar to **8** in the solid state.⁸⁴ While the bonding observed in **8** is not novel, this structure serves as an example to showcase the reactivity and coordination of knicnac.



Scheme 20: Synthesis of *bis*(knicnac)zinc, **8**.

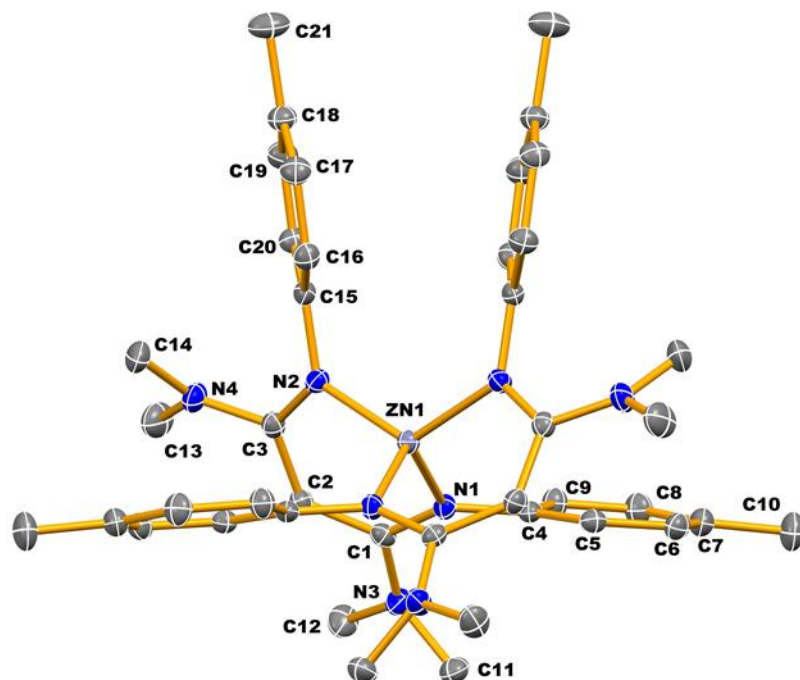


Figure 22: Solid state structure of *bis*(knicnac)zinc, **8**. Only the atoms that are crystallographically unique have been labeled; the other half of the molecule is generated by rotation about a two-fold axis. Thermal ellipsoids are drawn at the 50 % probability level. Hydrogen atoms have been omitted for clarity.

Chapter 3 – Summary & Conclusions

Two, new, electron-rich 1,3-diketiminato ligands have been prepared and fully characterized. Although the desired boron carbenoid was not produced in the reactions of nocnoc and a variety of boron-containing species, DFT and MP2 calculations predicted that the ground state of such a complex is a singlet. The singlet-to-triplet energy gap may be sufficiently large enough for the isolation of a low-valent boron analogue. Further investigations into the reactivities of these ligands have also been started. The study of their coordination complexes will add to the fundamental understanding of such inorganic systems. A “steric clash” has also been identified and shown to cause a boat-type conformation being adopted in some inorganic heterocycles. It has also been proven that these ligands can stabilize reactive species for long periods of time, even preventing hydrolysis. This is likely due to their “bowl-shaped” pocket, as well as their strong donor properties to the metal centre. Finally, π -type Zn \cdots C interactions, which are likely weak and electrostatic in nature, but may be structurally important, have been identified.

Chapter 4 – Future Work

Both ligands reported in this work should be investigated further in attempts to prepare a boron analogue of a carbene. Although computations indicated that the *p*-tolyl substituent should have provided the largest singlet-to-triplet energy gap, attempts should be made to prepare either the 2,6-diisopropylphenyl or 2,4,6-trimethylphenyl substituted ligand species. Both of these substituents may offer a better “bowl-shaped” pocket to prevent self-oligomerization and may assist with solid state stabilization. 4-methoxyphenyl or 4-aminophenyl substituents should also be investigated as possible ligand side chains; their increased donation abilities may increase the stabilization of the singlet state. Varying the substitution at the R³ (α -) position should also be investigated computationally, to determine if strategic functionalization at this position can yield a large singlet-to-triplet energy gap. Finally, future attempts to prepare boron analogues should use cyclohexane as the reaction solvent since it has been shown, computationally, that they can undergo C–H bond insertion; it should be thermodynamically unfavourable to break the cyclic ring of cyclohexane.

The work presented here is only a brief introduction to the potential reactivity of these ligands. Ideally, these ligands should be reacted with other transition metal and main-group complexes to truly study their properties. It would also be interesting to prepare a lanthanoid complex to determine the ligand’s bite angle. Finally, both of these ligands’ substitution patterns are similar to BOX-type ligands, and therefore their organometallic complexes should be stable in the presence of strong bases. If this could be proven to be true, then catalysts that incorporate these ligands should be prepared and studied.

Chapter 5 – Experimental

5.1 General Procedures

All preparations were performed under an inert nitrogen atmosphere in either an mBraun glove box or using standard Schlenk line techniques,⁷² unless otherwise stated. Nitrogen (>99.998%) and carbon dioxide (50% in nitrogen) were provided by Praxair Inc. Diethyl malonimidate dihydrochloride, *p*-toluidine (99.6%), malononitrile ($\geq 99\%$), dichloromethylene-dimethyliminium chloride (Viehe's salt,⁶⁹ technical grade), potassium hydride, potassium hydroxide, ethanol ($\leq 0.003\%$ H₂O), anhydrous 1,4-dioxane (99.8%), 1,2-dimethoxyethane (99.5%), anhydrous diethyl ether ($\geq 99.0\%$), deuterium oxide (D: 99.9%), boron trifluoride diethyl etherate, boron tribromide ($\geq 99.99\%$), hydrogen chloride solution (4.0 M in 1,4-dioxane), trimethylaluminum solution (2.0 M in heptane), diethylzinc solution (1.0 M in hexanes), boron trichloride solution (1.0 M in hexanes) and methylmagnesium bromide solution (3.0 M in diethyl ether) were purchased from Sigma-Aldrich and were used without further purification. Hyflo Super Cel[®] (Celite) and naphthalene (99%) were also purchased from Sigma-Aldrich and were dried in a vacuum oven prior to use. Granular lithium (99%) and potassium (98.5%) were purchased from Sigma-Aldrich, and were finely divided and rinsed with dry hexanes prior to use. The chlorodicarbonylrhodium(I) dimer was purchased from Strem Chemicals Inc. Reagent grade ethylacetate, hexanes, heptane, toluene, dichloromethane and THF were supplied by Caledon Laboratory Chemicals. Heptane, hexanes, toluene and THF were purified using an mBraun MB-SPS-800 solvent purification system and were stored over 4 Å molecular sieves prior to use. Silica gel (60-200 mesh), magnesium sulfate, and potassium bromide (infrared grade) were purchased from Fisher Scientific, the silica was used as received

without drying, and the KBr and MgSO₄ were dried/stored in an oven prior to use. Benzene-D₆ (D: 99.5%) and DMSO-D₆ (D: 99.9%) were purchased from Cambridge Isotope Laboratories, Inc. and were opened/stored under nitrogen. Potassium-graphite was prepared following a known literature method.⁷⁰

5.2 Spectroscopic & Characterization Techniques

The infrared spectra of **2** and **8** were obtained using an attenuated total reflection (ATR) adapter on a Bruker Alpha Spectrometer. All other infrared spectra were collected as KBr pellets using a Bruker Vertex 70 Infrared Spectrometer. Data processing was completed using OPUS 6.0 software suite.

The NMR experiments were carried out on either a Bruker Ultrashield 300 MHz NMR spectrometer with a 7.05 Tesla magnet. The NMR data for **5** was collected on a Bruker AV 500 MHz Spectrometer, with an 11.74 Tesla magnet, at the Nuclear Magnetic Resonance Research Resource (NMR-3) facility at Dalhousie University in Halifax, Nova Scotia. The samples were prepared by dissolving a small amount of the compound into an aliquot of the deuterated solvent under an inert atmosphere. ¹H and ¹³C{¹H} spectra were referenced to residual solvent downfield of trimethylsilane. Peaks were assigned by considering results from COSY, HSQC and DEPTQ experiments, as well as by relative integration in the ¹H spectra. The data was processed using Bruker TOPSIN 1.3.

Elemental analyses (EA) were performed on a Perkin Elmer CHN Analyzer 2400 Series II. Prior to data acquisition standard calibration was conducted with acetanilide supplied by Perkin Elmer. High resolution mass spectrometry (positive mode) analysis was performed on a Bruker microTOF Focus Mass Spectrometer by the method of atmospheric-pressure chemical ionization in methanol. All EA data acquisition was obtained by Patricia

Granados of the Centre for Environmental Analysis and Remediation at Saint Mary's University. The HRMS data was collected by Xiao Feng of the Maritime Mass Spectrometry Laboratories at Dalhousie University in Halifax, Nova Scotia.

The melting points were measured using a Mel-Temp melting point apparatus (with a heating rate of $\sim 5\text{ }^{\circ}\text{C min}^{-1}$) and are uncorrected. The samples were prepared by filling a capillary tube with few milligrams of sample material and sealing the tube under an inert atmosphere.

The real-time analysis of **6** was performed using a Mettler-Toledo ReactIR 15 spectrometer equipped with a silicon-tipped probe. To accurately monitor the rate of a reaction, the reagents and products must be fully soluble in the reaction solvent; for this reason, DCM was chosen as the solvent. NocNoc (0.13 g, 0.38 mmol) was dissolved in 3 mL of DCM in a 20 mL Schlenk tube equipped with a stir bar and the ReactIR probe. The flask was continuously purged with nitrogen as the trimethylaluminum solution (0.50 mL, 2.0 M in heptane) was added to the flask. **Caution!** *Trimethylaluminum is pyrophoric and appropriate procedures must be followed when handling outside of a glove box.* The C=N absorption of NocNoc, at 1667 cm^{-1} , immediately disappeared, and the C–N absorption of **6**, 1436 cm^{-1} , appeared within 15 seconds. The reaction was monitored for 10 minutes, with the absorption peak at 1436 cm^{-1} reaching a maximum by 1 minute. The volatiles were removed *in vacuo* and NMR analysis confirmed the identity of **6**. The spectra were recorded at 15 s intervals and iC.IR 4.3 software was used for data processing.

The phase transitions in **6** were determined by differential scanning calorimetry using a TA Instruments' DSC Q100. The DSC was calibrated at the melting point of indium metal ($156.6\text{ }^{\circ}\text{C}$), for both heating rates used. A few crystals of **6** (4.7 mg) were placed in

an aluminum pan which was hermetically sealed. The sample was held isothermally at -80 °C for 5 minutes, then the sample was heated to 170 °C at a rate of 10 °C min⁻¹. The sample was then held for a second isotherm of 170 °C for 3 minutes before being cooled to -80 °C at 10 °C min⁻¹. It was found that the sample's thermal history had an effect on its thermal behaviour. After being held at -80 °C for 3 minutes, the sample was then reheated to 170 °C at a rate of 20 °C min⁻¹, followed by cooling back to -80 °C at the same rate. The enthalpies of the transitions were output in units of J g⁻¹, however, for consistency, these were converted to units of kJ mol⁻¹, using the molar mass of **6**, and Equation 4. TA Universal Analysis 2000 was used for data processing and the DSC curve was plotted with Microsoft Office Excel 2013. Instrumentation was provided by Dr. Kathy Singfield of the Department of Chemistry at Saint Mary's University.

$$1 \text{ J g}^{-1} = 0.3940 \text{ kJ mol}^{-1} \quad (4)$$

5.3 Gaseous HCl-free Synthesis of Diethyl Malonimidate Dihydrochloride

Malononitrile (7.35 g, 0.11 mol), *anhydrous* ethanol (13.5 mL, 0.23 mol), and 30 mL of 1,4-dioxane were added to a 250 mL Schlenk flask which was fully submerged in ice. A solution of hydrogen chloride (56.0 mL, 4.0 M in 1,4-dioxane) was slowly added to the flask and it was left to stir for 18 hours between 0 and 5 °C. After stirring, the off-white suspension was filtered through a sintered glass frit and the solids were rinsed with *ca.* 10 mL of cold diethyl ether. The resulting beige powder was collected and dried under vacuum for 12 hours. Yield = 21.97 g (86 % based upon consumption of malononitrile). Spectroscopic data is consistent with that found in the literature.^{66,67} mp = 122 °C. ¹H (300 MHz, DMSO-D₆, ppm): 1.28 (t, 6H, ³J_{CH} = 7.11 Hz, -OCH₂CH₃), 4.12 (q, 4H, ³J_{CH} = 7.12 Hz, -OCH₂CH₃), 4.22 (br s, 2H, HCl), 4.52 (br s, 2H, CH₂), 7.51 (t, 2H, ¹J_{NH} = 50.78 Hz,

=NH). $^{13}\text{C}\{^1\text{H}\}$ (75 MHz, DMSO- D_6 , ppm): 14.07 (s, $-\text{OCH}_2\text{CH}_3$), 42.40 (s, CH_2), 60.82 (s, $-\text{OCH}_2\text{CH}_3$), 169.11 (s, $\text{N}=\text{C}$). IR (KBr, cm^{-1}): 3000 (vs, br), 1736 (vs), 1672 (vs), 1575 (m), 1445 (vs), 1405 (vs), 1364 (s), 1300 (m), 1206 (w), 1136 (m), 1093 (m), 1032 (w), 1004 (m), 950 (m), 901 (m), 868 (w), 823 (m), 808 (w), 634 (m), 447 (w).

5.4 Synthesis of NocNoc, 2

Diethyl malonimidate dihydrochloride (2.5 g, 10.8 mmol) and excess *p*-toluidine (3.5 g, 32.7 mmol) were added to *ca.* 50 mL of THF and it was set to reflux for 18 hours, under nitrogen, resulting in a yellow suspension. (*Note: the following steps were performed on the benchtop, not under an inert atmosphere*). The precipitate was removed by vacuum filtration and the filtrate was collected. The supernatant was removed by vacuum resulting in an orange oil. This was subsequently purified by passing it through a silica packed column with a 20:1, hexanes: ethylacetate, solution as the eluent. The first fraction was collected and the solvent was removed under vacuum resulting in a pale yellow oil. Yield = 1.1 g (30 % based upon consumption of DEMHCl). Clear, colourless, crystals were obtained from the oil after letting it sit at 5 °C for one week. mp = 42 °C. ^1H (300 MHz, C_6D_6 , ppm): 1.16 (t, 6H, $^3J_{\text{CH}} = 7.09$ Hz, $-\text{OCH}_2\text{CH}_3$), 2.15 (s, 6H, $-\text{ArCH}_3$), 3.09 (s, 2H, CH_2), 4.21 (q, 4H, $^3J_{\text{CH}} = 7.10$ Hz, $-\text{OCH}_2\text{CH}_3$), 6.67 (d, 4H, $^3J_{\text{CH}} = 8.21$ Hz, Ar), 6.95 (d, 4H, $^3J_{\text{CH}} = 7.91$ Hz, Ar). $^{13}\text{C}\{^1\text{H}\}$ (75 MHz, C_6D_6 , ppm): 14.24 (s, $-\text{OCH}_2\text{CH}_3$), 20.85 (s, $-\text{ArCH}_3$), 31.67 (s, CH_2), 61.95 (s, $-\text{OCH}_2\text{CH}_3$), 121.41 (s, Ar), 129.87 (s, Ar), 132.23 (s, Ar), 146.68 (s, Ar), 157.66 (s, $\text{N}=\text{C}$). IR (ATR, cm^{-1}): 2978 (w), 2940 (w), 2926 (w), 2900 (w), 1660 (vs), 1612 (w), 1507 (m), 1311 (m), 1222 (s), 1171 (m), 1038 (s), 864 (m), 831 (m), 804 (m), 534 (m). EA calcd. [%]: C, 74.52; H, 7.74; N, 8.28; found [%]: C, 74.07; H, 7.61; N, 8.25. HRMS calcd. [m/z]: 339.2028; found [m/z]: 339.2074.

5.5 Synthesis of KnicNac, 3

Dimethylacetamide (2.25 g, 25.83 mmol) was added to a solution of Viehe's salt⁶⁹ (8.40 g, 51.71 mmol) in *ca.* 75 mL of DCM and it was set to reflux for 3 hours, followed by the dropwise addition of a *p*-toluidine (7.0 g, 65.33 mmol) solution in *ca.* 30 mL of DCM. After refluxing for another 6 hours, the solution was transferred to a separatory funnel with an additional 100 mL of water and 100 mL of DCM. The DCM layer was drained and potassium hydroxide was added to the aqueous layer until a pH of ~12 was reached. Three, 50 mL portions of DCM were added to the separatory funnel and the DCM layer was collected after each addition. Magnesium sulfate was added to the collected DCM extractions to remove residual water and the resulting suspension was filtered by gravity. The volatiles of the filtrate were removed *in vacuo*, and the crude product was further purified by column chromatography with a silica packed column. (*Note: the silica was rinsed with a hexanes solution containing 2% trimethylamine and 5% ethylacetate*). A 20:1 hexanes: ethylacetate solution was used as the eluent until the first fraction passed through the column, then ethylacetate was used to elute the second fraction, which was collected, and placed under vacuum, resulting in the isolation of an orange solid. Yield = 4.78 g (55% based upon consumption of dimethylacetamide). Orange, needle-shaped, crystals were obtained by slow evaporation of a saturated diethyl ether solution. This synthesis was achieved with considerable assistance from Bright Huo, Jetsuda Areephong, and Dr. Kai Ylijoki of the Department of Chemistry at Saint Mary's University. mp = 107 °C. ¹H (300 MHz, C₆D₆, ppm): 2.20 (s, 6H, -ArCH₃), 2.70 (s, 12H, -NCH₃), 3.56 (s, 2H, CH₂), 6.64 (d, 4H, ³J_{CH} = 8.15 Hz, Ar), 7.01 (d, 4H, ³J_{CH} = 7.94 Hz, Ar). ¹³C{¹H} (75 MHz, C₆D₆, ppm): 20.87 (s, -NCH₃), 28.98 (br s, CH₂), 38.26 (s, -ArCH₃), 122.74 (s, Ar), 129.94 (s,

Ar), 130.78 (s, Ar), 149.23 (s, Ar), 155.71 (s, N=C). IR (KBr, cm^{-1}): 3020 (w), 2917 (m), 1602 (vs), 1481 (m), 11411 (m), 1382 (s), 1293 (m), 1195 (m), 1168 (m), 1134 (m), 1106 (m), 1059 (m), 980 (w) 846 (w), 822 (w). HRMS calcd. [m/z]: 337.2348; found [m/z]: 337.2389.

5.6 Deuterium Exchange Study

A 0.05 M solution of potassium hydroxide was prepared by dissolving 0.0105 g of KOH in 4.0 mL of deuterium oxide. A small amount of **2** (0.0175 g, 0.0518 mmol) was dissolved in of mixture consisting of 2 mL of D_2O , 1 mL of 1,4-dioxane, and 60 μL of the KOH/ D_2O solution. The solution was stirred in a sand bath at 50 $^\circ\text{C}$ for 18 hours, resulting in a pale yellow suspension. The supernatant was removed *via* vacuum filtration and an off-white powder was isolated. The same process was repeated for KnicNac using 0.0189 g (0.0563 mmol) of **3**.

2· D_2 : ^1H (300 MHz, C_6D_6 , ppm): 1.15 (t, 6H, $^3J_{\text{CH}} = 7.08$ Hz, $-\text{OCH}_2\text{CH}_3$), 2.14 (s, 6H, $-\text{ArCH}_3$), 4.25 (q, 4H, $^3J_{\text{CH}} = 7.10$ Hz, $-\text{OCH}_2\text{CH}_3$), 6.76 (d, 4H, $^3J_{\text{CH}} = 8.20$ Hz, Ar), 6.97 (d, 4H, $^3J_{\text{CH}} = 7.92$ Hz, Ar).

3· D_2 : ^1H (300 MHz, C_6D_6 , ppm): 2.20 (s, 6H, $-\text{ArCH}_3$), 2.70 (s, 12H, $-\text{NCH}_3$), 6.65 (d, 4H, $^3J_{\text{CH}} = 8.15$ Hz, Ar), 7.02 (d, 4H, $^3J_{\text{CH}} = 7.97$ Hz, Ar).

5.7 Synthesis of the Rhodium Carbonyl Complex of nocnoc, **4**

A suspension of potassium hydride (0.0306 g, 0.8976 mmol) in *ca.* 2 mL of THF was slowly added to a solution of **2** (0.1046 g, 0.3091 mmol) in *ca.* 3 mL of THF and the resulting solution was allowed to stir for 2 hours. After stirring, the orange solution was filtered through Celite and a solution of chlorodicarbonylrhodium(I) dimer (0.0601 g, 0.1546 mmol) in *ca.* 2 mL of THF was added dropwise to the filtrate. After stirring for 18

hours the supernatant was removed *in vacuo* and the solids were rinsed with *ca.* 8 mL of toluene. The solution was filtered through Celite and placed in a -35 °C freezer for several days resulting in the formation of a single orange crystal. Yield = 0.0450 g (70 % based upon consumption of **2**). mp = 158 °C. ^1H (300 MHz, C_6D_6 , ppm): 0.81 (t, 6H, $^3J_{\text{CH}} = 6.97$ Hz, $-\text{OCH}_2\text{CH}_3$), 2.12 (s, 6H, $-\text{ArCH}_3$), 3.52 (q, 4H, $^3J_{\text{CH}} = 6.97$ Hz, $-\text{OCH}_2\text{CH}_3$), 4.14 (s, 1H, CH), 7.01 (d, 4H, $^3J_{\text{CH}} = 7.89$ Hz, Ar), 7.29 (d, 4H, $^3J_{\text{CH}} = 8.16$ Hz, Ar). $^{13}\text{C}\{^1\text{H}\}$ (75 MHz, C_6D_6 , ppm): 14.48 (s, $-\text{OCH}_2\text{CH}_3$), 20.94 (s, $-\text{ArCH}_3$), 63.59 (s, CH), 64.83 (s, $-\text{OCH}_2\text{CH}_3$), 126.49 (s, Ar), 128.86 (s, Ar), 134.04 (s, Ar), 153.76 (s, Ar), 166.10 (s, $\text{N}=\text{C}$), 185.08 (d, $^1J_{\text{RhC}} = 66.30$ Hz, $-\text{RhC}=\text{O}$). IR (KBr, cm^{-1}): 3414 (m, br), 2984 (w), 2056 (vs), 1988 (vs), 1573 (s), 1538 (s), 1503 (s), 1475 (s), 1425 (s), 1311 (s), 1297 (m), 1199 (s), 1118 (m), 1082 (m), 852 (m). EA caclcd. [%]: C, 55.65; H, 5.08; N, 5.64; found [%]: C, 55.22; H, 4.83; N, 5.55.

5.8 Synthesis of the Rhodium Carbonyl Complex of knicnac, **5**

A solution of **3** (0.0431 g, 0.1281 mmol) in *ca.* 1 mL of THF was added to a suspension of potassium hydride (0.0101 g, 0.2518 mmol) in *ca.* 2 mL of THF and the resulting solution was left to stir for 2 hours. The orange solution was filtered through Celite and a solution of chlorodicarbonylrhodium(I) dimer (0.0249 g, 0.0640 mmol) in *ca.* 2 mL of THF was added dropwise to the filtrate. The dark red solution was stirred for 18 hours before the volatiles were removed under vacuum, then *ca.* 4 mL of toluene was added to the residual solids. The solution was filtered through Celite and the filtrate was placed in a -35 °C freezer for 2 days. This gave small, yellow, cubic, crystals, which were isolated by filtration. Yield = 0.0212 g (33 % based upon consumption of **3**). ^1H (500 MHz, C_6D_6 , ppm): 2.08 (s, 6H, $-\text{ArCH}_3$), 2.35 (s, 12H, $-\text{NCH}_3$), 4.15 (s, 1H, CH), 6.90 (d, 4H, $^3J_{\text{CH}} =$

7.55 Hz, Ar), 7.04 (d, 4H, $^3J_{\text{CH}} = 7.77$ Hz, Ar). $^{13}\text{C}\{^1\text{H}\}$ (125 MHz, C_6D_6 , ppm): 20.77 (s, $-\text{Ar}\underline{\text{C}}\text{H}_3$), 40.57 (s, $-\text{N}\underline{\text{C}}\text{H}_3$), 81.27 (s, $\underline{\text{C}}\text{H}$), 123.95 (s, Ar), 124.43 (s, Ar), 129.43 (s, Ar), 130.16 (s, Ar), 165.97 (s, $\text{N}=\underline{\text{C}}$), 187.24 (d, $^1J_{\text{RhC}} = 69.85$ Hz, $-\text{Rh}\underline{\text{C}}\text{O}$). IR (KBr, cm^{-1}): 3020 (w), 2990 (w), 2918 (m), 2866 (w), 2049 (vs), 1977 (vs), 1607 (vs), 1526 (vs), 1502 (vs), 1420 (s), 1388 (s), 1326 (vs), 1261 (m), 1225 (w), 1184 (m), 1159 (m), 1119 (w), 1034 (m), 820 (w).

5.9 Synthesis of the Dimethylaluminum Complex of nocnoc, **6**

A solution of trimethylaluminium (0.65 mL, 2.0 M in heptane) was slowly added to a solution of **2** (0.22 g, 0.65 mmol) in *ca.* 2 mL of heptane. The solution immediately began to bubble and produce a white precipitate. After *ca.* 10 minutes the resulting yellow supernatant was decanted and the precipitate was rinsed three times with 1 mL portions of heptane. The precipitate was dissolved in *ca.* 3 mL of THF and was left to recrystallize by slow evaporation. This gave a single colourless, large, block-shaped, crystal. Yield = 0.18 g (71 % based upon consumption of **2**). A small amount (~10 mg) of **6** was removed from an inert atmosphere and was left open to ambient conditions during the preparation of this thesis (~8 months). After this exposure, the sample was determined to still be **6**; hydrolysis/degradation products were not observed. mp = 158 °C. ^1H (300 MHz, C_6D_6 , ppm): -0.25 (s, 6H, $-\text{Al}\underline{\text{C}}\text{H}_3$), 0.81 (t, 6H, $^3J_{\text{CH}} = 7.08$ Hz, $-\text{OCH}_2\underline{\text{C}}\text{H}_3$), 2.08 (s, 6H, $-\text{Ar}\underline{\text{C}}\text{H}_3$), 3.49 (q, 4H, $^3J_{\text{CH}} = 7.08$ Hz, $-\text{OCH}_2\underline{\text{C}}\text{H}_3$), 3.95 (s, 1H, $\underline{\text{C}}\text{H}$) 6.99 (d, 4H, $^3J_{\text{CH}} = 8.01$ Hz, Ar), 7.23 (d, 4H, $^3J_{\text{CH}} = 8.27$ Hz, Ar). $^{13}\text{C}\{^1\text{H}\}$ (75 MHz, C_6D_6 , ppm): 14.22 (s, $-\text{OCH}_2\underline{\text{C}}\text{H}_3$), 20.95 (s, $-\text{Ar}\underline{\text{C}}\text{H}_3$), 61.89 (s, $\underline{\text{C}}\text{H}$), 64.29 (s, $-\text{OCH}_2\underline{\text{C}}\text{H}_3$), 121.48 (s, $-\text{Al}\underline{\text{C}}\text{H}_3$), 126.95 (s, Ar), 129.69 (s, Ar), 134.57 (s, Ar), 140.65 (s, Ar), 168.41 (s, $\text{N}=\underline{\text{C}}$). IR (KBr, cm^{-1}): 3474 (w, br), 3029 (w), 2983 (m), 2919 (m), 1891 (w), 1677 (m), 1571 (vs), 1537

(vs), 1506 (s), 1439 (vs), 1376 (m), 1319 (vs), 1209 (s), 1181(m), 1095 (m), 855 (m), 745 (m), 703 (m), 670 (m), 513 (m). EA calcd. [%]: C, 70.03; H, 7.92; N, 7.10; found [%]: C, 69.91; H, 7.74; N, 7.09.

5.10 Synthesis of the Ethylzinc Complex of nocnoc, 7

A solution of diethylzinc (1.06 mL, 1.0 M in hexanes) was slowly added to a solution of **2** (0.18 g, 0.53 mmol) in *ca.* 3 mL of hexanes, without stirring. After addition, the yellow solvent was removed by slow evaporation over several hours, giving large, colourless, block-shaped, crystals. Yield = 0.20 g (87 % based upon consumption of **2**). mp = 189-191 °C (dec). ^1H (300 MHz, C_6D_6 , ppm): 0.51 (q, 2H, $^3J_{\text{CH}} = 8.12$ Hz, $-\text{ZnCH}_2\text{CH}_3$), 0.93 (t, 6H, $^3J_{\text{CH}} = 7.02$ Hz, $-\text{OCH}_2\text{CH}_3$), 1.22 (t, 3H, $^3J_{\text{CH}} = 8.12$ Hz, $-\text{ZnCH}_2\text{CH}_3$), 2.14 (s, 6H, $-\text{ArCH}_3$), 3.64 (q, 4H, $^3J_{\text{CH}} = 7.02$ Hz, $-\text{OCH}_2\text{CH}_3$), 4.12 (s, 1H, CH), 7.03 (d, 4H, $^3J_{\text{CH}} = 8.16$ Hz, Ar), 7.11 (d, 4H, $^3J_{\text{CH}} = 8.34$ Hz, Ar). $^{13}\text{C}\{^1\text{H}\}$ (75 MHz, C_6D_6 , ppm): 12.73 (s, $-\text{ZnCH}_2\text{CH}_3$), 14.82 (s, $-\text{OCH}_2\text{CH}_3$), 21.27 (s, $-\text{ArCH}_3$), 63.02 (s, CH), 64.40 (s, $-\text{OCH}_2\text{CH}_3$), 126.13 (s, Ar), 129.60 (s, Ar), 132.14 (s, $-\text{ZnCH}_2\text{CH}_3$), 133.27 (s, Ar), 144.85 (s, Ar), 167.34 (s, $\text{N}=\text{C}$). IR (KBr, cm^{-1}): 3620 (w), 3021 (w), 2980 (m), 2927 (m), 2896 (m), 2850 (m), 1663 (m), 1577 (vs), 1526 (s), 1503 (vs), 1446 (vs), 1438 (vs), 1371 (s), 1286 (s), 1266 (s), 1201 (m), 1191 (s), 1113 (m), 1075 (s), 1017 (m), 985 (m), 848 (m), 809 (m), 742 (m), 583 (m), 518 (m), 510 (m). EA calcd. [%]: C, 63.96; H, 7.00; N, 6.49; found [%]: C, 62.14; H, 6.70; N, 6.31.

5.11 Synthesis of Bis(knicnac)zinc, 8

A solution of diethylzinc (0.30 mL, 1.0 M in hexanes) was slowly added to a solution of **3** (0.0664 g, 0.1976 mmol) in 5 mL of a 1:1 solution of hexanes and heptane. The solution was briefly stirred by hand and the clear/colourless solution was then placed

in a -15 °C freezer for one week. This resulted in the formation of pale yellow, needle-shaped, crystals. Yield = 0.0480 g (66 % based upon consumption of **3**). mp = 135 °C. ^1H (300 MHz, C_6D_6 , ppm): 2.10 (s, 12H, $-\text{ArCH}_3$), 2.46 (s, 24H, $-\text{NCH}_3$), 4.14 (s, 2H, CH), 6.80 (d, 8H, $^3J_{\text{CH}} = 8.18$ Hz, Ar), 6.92 (d, 8H, $^3J_{\text{CH}} = 8.28$ Hz, Ar). $^{13}\text{C}\{^1\text{H}\}$ (75 MHz, C_6D_6 , ppm): 20.87 (s, $-\text{ArCH}_3$), 40.95 (s, $-\text{NCH}_3$), 77.30 (s, CH), 122.72 (s, Ar), 123.75 (s, Ar), 129.14 (s, Ar), 126.62 (s, Ar), 166.61 (s, $\text{N}=\text{C}$). IR (ATR, cm^{-1}): 2919 (w), 2859 (w), 1594 (m), 1498 (vs), 1404 (vs), 1370 (s), 1320 (s), 1262 (m), 1169 (s), 1100 (m), 1024 (s), 805 (s), 497 (m).

5.12 Computational Details

All calculations/graphical images were performed/generated using the Spartan '14 software package,⁶¹ unless otherwise stated. All *ab initio* computations performed by Spartan were first drawn using the graphical interface, followed by computing the equilibrium conformation *via* semi-empirical (PM3)⁸⁵ methods. The lowest energy conformations were then used as the initial geometries for DFT calculations of the equilibrium geometry at the B3LYP^{86,87} level of theory, using the 6-31G* basis set. Vibrational frequency calculations were performed on all structures to confirm that the geometries were in fact a minimum (imaginary frequencies = 0). All second order Møller-Plesset (MP2)^{88,89} calculations were performed by first computing the equilibrium conformation (PM3) in Spartan, as described above, followed by geometry optimizations at the MP2/6-31G* level of theory using Gaussian 09 Rev. C.01.⁹⁰ For computational efficiency, aryl substituents for all MP2 level calculations were replaced with phenyls. The singlet triplet energy gaps were determined using Equation 1. Computational facilities for

all calculations performed with Gaussian were provided by ACEnet, the regional high performance computing consortium for universities in Atlantic Canada.

$$\Delta E_{\text{st}} = E_{\text{Triplet}} - E_{\text{Singlet}} \quad (\mathbf{1a})$$

$$1 \text{ Ha} = 2625.5 \text{ kJ mol}^{-1} \quad (\mathbf{1b})$$

To determine if the ground-state singlet was open or closed-shell, the singlet-state was recalculated using the unrestricted SCF (UB3LYP). The α and β electrons were allowed to mix, and the optimized wavefunction converged to the same energy, and electronic configuration, as computed for the closed-shell singlet; spin contamination, $\langle S^2 \rangle = 0.0001$. The thermodynamics of the singlet state carbenoid (**1s**), and its dimer (**1d**), were computed from their optimized wave-functions at the B3LYP/6-31G* level of theory.

The geometry optimizations for the rhodium carbonyl complexes were performed at the B3LYP/LANL2DZ level of theory, using the single crystal X-ray structures to provide the initial geometries. The LANL2DZ basis set was chosen because rhodium is not defined within the 6-31G* basis set. The theoretical infrared spectra for the optimized structures were also generated at the same level of theory. The CIF for (nacnac)Rh(CO)₂ was retrieved from the Cambridge Structural Database;³⁹ CCDC# 814889.

The nature of the bond between the monomer units of **7** was probed *via* a QTAIM^{78,79} analysis. DFT geometry optimizations were performed at the B3LYP, M06,⁹¹ and ω B97X-D⁹² levels of theory with the 6-31G* basis set as implemented in Gaussian 09 using the single crystal X-ray structure to provide the initial geometry. The B3LYP/6-31G* geometry best reproduced the crystal data, with M06 and ω B97X-D showing significant distortions of the ethyl group on zinc. The optimized wavefunction was then subjected to QTAIM analysis *via* the AIMAll software package.⁸² The computational investigation of

7 was performed by Iffenna Mbaezue and Dr. Kai Ylijoki of the Department of Chemistry at Saint Mary's University.

5.13 X-ray Crystallographic Details

All X-ray crystallographic analyses were performed by Dr. Katherine Robertson at Saint Mary's University, and all crystallographic diagrams presented within were prepared using Mercury CSD 3.6.⁹³

The crystal chosen for each determination was attached to the tip of a 400 μm MicroLoop with paratone-N oil. Measurements were made on a Bruker APEXII CCD equipped diffractometer (30 mA, 50 kV) using monochromated Mo $K\alpha$ radiation ($\lambda = 0.71073 \text{ \AA}$) at 125 K, except for the room temperature data collection which was carried out at 26 $^{\circ}\text{C}$.⁹⁴ The initial orientation and unit cell were indexed using a least-squares analysis of a random set of reflections collected from three series of 0.5° ω -scans, 15 seconds per frame and 12 frames per series, that were well distributed in reciprocal space. For data collection, four ω -scan frame series were collected with 0.5° wide scans, 30 second frames and 366 frames per series at varying ϕ angles ($\phi = 0^{\circ}, 90^{\circ}, 180^{\circ}, 270^{\circ}$). The crystal to detector distance was set to 6 cm and a complete sphere of data was collected. Cell refinement and data reduction were performed with the Bruker SAINT software,⁹⁵ which corrects for beam inhomogeneity, possible crystal decay, Lorentz and polarisation effects. A multi-scan absorption correction was applied (SADABS).⁹⁶ The structures were solved using either SHELXT-2014⁹⁷ or SHELXS-2014⁹⁷ and were refined using a full-matrix least-squares method on F^2 with SHELXL-2014.⁹⁷ All refinements were unremarkable. The non-hydrogen atoms were refined anisotropically. Hydrogen atoms bonded to carbon were included at geometrically idealized positions and were not refined.

The isotropic thermal parameters of the hydrogen atoms were fixed at $1.2U_{\text{eq}}$ of the parent carbon atom or $1.5U_{\text{eq}}$ for methyl hydrogens. In certain cases a disordered model was found to be best for methyl groups showing rotational motion. Such groups were best defined using an idealized disordered model with two sets of equally occupied positions, rotated from each other by 60 degrees. Each hydrogen in a disordered group was thus given an occupancy of 0.5.

The crystal used in the low temperature data collection of the dimethylaluminum complex of nocnoc, **6**, was found to be twinned. The initial unit cell determination located an orthorhombic unit cell. When the cell was refined after data collection, a primitive orthorhombic cell with dimensions, $a = 8.701(8)$, $b = 12.274(11)$ and $c = 21.910(19)$ was obtained. The merging R value for the orthorhombic unit cell was 0.097, while the merging R for a monoclinic unit cell with a Laue symmetry of $(1\ 1\ 2/m)$ was only 0.059 (the merging R values for the other two possible monoclinic orientations $(2/m\ 1\ 1)$ and $(1\ 2/m\ 1)$ were 0.095). Based on these results the unit cell appeared to truly be monoclinic (pseudomerohedral twinning with the monoclinic angle close to 90° , thus approximating an orthorhombic unit cell) and the data was reprocessed as such. The data was then transformed using the matrix $[1\ 0\ 0\ 0\ 0\ 1\ 0\ 1\ 0]$ to give a monoclinic unit cell with the unique axis b and cell dimensions, $a = 8.6122(12)$, $b = 21.6550(29)$, $c = 12.1405(16)$ and $\beta = 90.039(2)$. The systematic absences suggested the space group $P2_1/c$ (#14) and a reasonable structure solution could be obtained in this space group. The statistics for the data set were now as expected, $2\theta_{\text{max}} = 54.77^\circ$, $R(\text{int}) = 0.0564$ and $R(\text{sigma}) = 0.0478$. TwinRotMax, as implemented in Platon,⁹⁸ was used to find the twin law required to complete the refinement, $[-1\ 0\ 0\ 0\ -1\ 0\ 0\ 0\ 1]$. Using an HKLF4 refinement in SHELXL

the BASF parameter refined to a value of 0.429(1). The final R-factor refined to 0.0415 for 4076 observed reflections and to 0.0589 using all 5078 reflections, with $wR2 = 0.0931$ for all data and $GoF = 1.033$.

References

1. Housecroft, C. E.; Sharpe, A. G. *Inorganic Chemistry*; Pearson: Harlow, England, 2012. pp 225-236, 887-889.
2. Abrams, M. B.; Scott, B. L.; Baker, R. T. *Organometallics* **2000**, *19*, 4944-4956.
3. Hardman, N. J.; Abrams, M. B.; Pribisko, M. A.; Gilbert, T. M.; Martin, R. L.; Kubas, G. J.; Baker, R. T. *Angew. Chem. Int. Ed.* **2004**, *43*, 1955-1958.
4. Jones, C. *Coord. Chem. Rev.* **2010**, *254*, 1273-1289.
5. Jayakumar, S.; Ishar, M. P. S.; Mahajan, M. P. *Tetrahedron* **2002**, *58*, 379-471.
6. Canal, J. P.; Ramnial, T.; Dickie, D. A.; Clubrune, J. A. C. *Chem. Commun.* **2006**, 1809.
7. Feldman, J.; McLain, S. J.; Parathasarathy, A.; Marshall, W. J.; Calabrese, J. C.; Arthur, S. D. *Organometallics* **1997**, *16*, 1514-1516.
8. Luca, O. R.; Crabtree, R. H. *Chem. Soc. Rev.* **2013**, *42*, 1440-1459.
9. Bourget-Merle, L.; Lappert, M. F.; Severn, J. R. *Chem. Rev.* **2002**, *102*, 3031-3066.
10. Lappert, M. F.; Liu, D. Netherlands Patent 9401515, 1994.
11. Gibson, V. C.; Maddox, P. J.; Newton, C.; Redshaw, C.; Solan, G. A.; White, A. J. P.; Williams, D. J. *Chem. Commun.* **1998**, 1651-1652.
12. Jazdzewski, B. A.; Holland, P. L.; Pink, M.; Young, V. G., Jr.; Spencer, D. J. E.; Tolman, W. B. *Inorg. Chem.* **2001**, *40*, 6097-6107.
13. Abdalla, J. A. B.; Riddlestone, I. M.; Tirfoin, R.; Aldridge, S. *Angew. Chem. Int. Ed.* **2015**, *54*, 5098-5102.
14. Ding, Y.; Hao, H.; Roesky, H. W.; Noltemeyer, M.; Schmidt, H. G. *Organometallics* **2001**, *20*, 4806-4811.
15. Basuli, F.; Huffman, J. C.; Mindiola, D. J. *Inorg. Chem* **2003**, *42*, 8003-8010.

16. Driess, M.; Yao, S.; Brym, M.; van Wüllen, C. *Angew. Chem. Int. Ed.* **2006**, *45*, 6730-6733.
17. Sarish, S. P.; Roesky, H. W.; John, M.; Ringe, A.; Magull, J. *Chem. Commun.* **2009**, 2390-2392.
18. Sarish, S. P.; Nekoueishahraki, B.; Jana, A.; Roesky, H. W.; Schulz, T.; Stalke, D. *Chem. -Eur. J.* **2011**, *17*, 890-894.
19. Yao, S.; Xiong, Y.; Driess, M. *Organometallics* **2011**, *30*, 1748-1767.
20. Arrowsmith, M.; Hill, M. S.; Kociok-Kohn, G.; MacDougall, D. J.; Mahon, M. F.; Mallov, I. *Inorg. Chem.* **2012**, *51*, 13408-13418.
21. Rasappan, R.; Laventine, D.; Reiser, O. *Coord. Chem. Rev.* **2008**, *252*, 702-714.
22. Wohler, F.; Liebig *J. Ann. Pharm.* **1832**, *3*, 249-282.
23. Ugai, T.; Tanaka, R.; Dokawa, T. *J. Pharm. Soc. Jpn.* **1943**, *63*, 269-300.
24. Breslow, R. J. *J. Am. Chem. Soc.* **1958**, *80*, 3719-3726.
25. Berkessel, A.; Elfert, S.; Yatham, V. R.; Neudorfl, J.; Schlorer, N. E.; Teles, J. H. *Angew. Chem. Int. Ed.* **2012**, *51*, 12370-12374.
26. Arduengo, A. J., III; Harlow, R. L.; Kline, M. *J. Am. Chem. Soc.* **1991**, *113*, 361-363.
27. Arduengo, A. J., III; Dias, H. V. R.; Harlow, R. L.; Kline, M. *J. Am. Chem. Soc.* **1992**, *114*, 5530-5534.
28. For selected reviews on the chemistry of NHCs see; (a) Hopkinson, M. N.; Richter, C.; Schedler, M.; Glorius, F. *Nature* **2014**, *510*, 485-496; (b) *N-Heterocyclic Carbenes: Effective Tools for Organometallic Synthesis*; Nolan, S. P., Ed.; Wiley-VCH: Weinheim, Germany, 2014.
29. Kim, Y.; Streitwieser, A. *J. Am. Chem. Soc.* **2002**, *124*, 5757-5761.

30. Alder, R. W.; Allen, P. R.; Williams, S. J. *J. Chem. Soc., Chem. Commun.* **1995**, 1267-1268.
31. Dixon, D. A.; Arduengo, A. J., III *J. Phys. Chem* **1991**, *94*, 4180-4182.
32. Asay, M.; Jones, C.; Driess, M. *Chem. Rev.* **2011**, *111*, 354-396.
33. Mizuhata, Y.; Sasamori, T.; Tokitoh, N. *Chem. Rev.* **2009**, *109*, 3479-3511.
34. Tuononen, H. M.; Roesler, R.; Dutton, J. L.; Ragoonna, P. J. *Inorg. Chem.* **2007**, *46*, 10693-10706.
35. Borpuzari, M. P.; Guha, A. K.; Kar, R. *Struct. Chem.* **2015**, *26*, 859-871.
36. Sundermann, A.; Reiher, M.; Schoeller, W. W. *Eur. J. Inorg. Chem.* **1998**, 305-310.
37. Schmidt, E. S.; Jockisch, A.; Schmidbaur, H. *J. Am. Chem. Soc.* **1999**, *121*, 9758-9759.
38. Cui, C.; Roesky, H. W.; Schmidt, H.; Noltemeyer, M.; Hao, H.; Cimpoesu, F. *Angew. Chem. Int. Ed.* **2000**, *39*, 4274-4276.
39. The Cambridge Crystallographic Data Centre (CCDC). <http://www.ccdc.cam.ac.uk>.
40. Hardman, N. J.; Eichler, B. E.; Power, P. P. *Chem. Commun.* **2000**, 1991-1992.
41. Hill, M. S.; Hitchcock, P. B. *Chem. Commun.* **2004**, 1818-1819.
42. Cheng, Y.; Hitchcock, P. B.; Lappert, M. F.; Zhou, M. *Chem. Commun.* **2005**, 752-754.
43. Hill, M. S.; Hitchcock, P. B.; Pongtavornpinyo, R. *Dalton Trans.* **2005**, 273-277.
44. Chen, C.; Tsai, M.; Su, M. *Organometallics* **2006**, *25*, 2766-2773.
45. Segawa, Y.; Yamashita, M.; Nozaki, K. *Science* **2006**, *314*, 113-115.
46. Jones, C.; Junk, P. C.; Platts, J. A.; Stasch, A. *J. Am. Chem. Soc.* **2005**, *128*, 2206-2207.
47. Findlater, M.; Hill, N. J.; Cowley, A. H. *Dalton Trans.* **2008**, 4419-4423.

48. Singlet-triplet energy gaps for boron carbenoids of nacnac have been previously reported with varying basis sets and aryl substituents. For consistency, the values presented herein were recalculated at the B3LYP/6-31G* and MP2/6-31G* levels of theory with Dipp and Ph substituents, respectively.
49. Kinjo, R.; Donnadieu, B.; Celik, M. A.; Frenking, G.; Bertrand, G. *Science* **2011**, *333*, 610-613.
50. Chang, M.; Otten, E. *Inorg. Chem.* **2015**, *54*, 8656-8664.
51. Doddi, A.; Prabusankar, G.; Gemel, C.; Winter, M.; Fischer, R. A. *Eur. J. Inorg. Chem.* **2013**, 3609-3615.
52. Ganesamoorthy, C.; Bendt, G.; Blaser, D.; Wolper, C.; Schulz, S. *Dalton Trans.* **2015**, *44*, 5153-5159.
53. Chu, T.; Boyko, Y.; Korobkov, I.; Nikonov, G. I. *Organometallics* **2015**, *34*, 5363-5365.
54. Hill, M. S.; Hitchcock, P. B.; Pongtavornpinyo, R. *Inorg. Chem.* **2007**, *46*, 3783-3788.
55. Ganesamoorthy, C.; Blaser, D.; Wolper, C.; Schulz, S. *Organometallics* **2015**, *34*, 2991-2996.
56. Lee, P. T. K. Saint Mary's University, Halifax, NS, 2009.
57. Kong, L.; Li, Y.; Ganguly, R.; Vidovic, D.; Kinjo, R. *Angew. Chem. Int. Ed.* **2014**, *53*, 9280-9283.
58. Kuhn, N.; Steimann, M.; Weyer, G. *Z. Naturforsch., B: Chem. Sci.* **1999**, *54b*, 427-433.
59. Murphy, L. J.; Robertson, K. N.; Kemp, R. A.; Tuononen, H. M.; Clyburne, J. A. C. *Chem. Commun.* **2015**, *51*, 3942-3956.
60. Feroci, M.; Chiarotto, I.; Forte, G.; Inesi, A. *J. CO2 Util.* **2013**, *2*, 29-34.

61. Shao, Y.; Molnar, L. F.; Jung, Y.; Kussmann, J.; Ochsenfeld, C.; Brown, S. T.; Gilbert, A. T. B.; Slipchenko, L. V.; Levchenko, S. V.; O'Neill, D. P.; DiStasio, R. A., Jr; Lochan, R. C.; Wang, T.; Beran, G. J. O.; Besley, N. A.; Herbert, J. M.; Yeh Lin, C.; Van Voorhis, T.; Hung Chien, S.; Sodt, A.; Steele, R. P.; Rassolov, V. A.; Maslen, P. E.; Korambath, P. P.; Adamson, R. D.; Austin, B.; Baker, J.; Byrd, E. F. C.; Dachsel, H.; Doerksen, R. J.; Dreuw, A.; Dunietz, B. D.; Dutoi, A. D.; Furlani, T. R.; Gwaltney, S. R.; Heyden, A.; Hirata, S.; Hsu, C.; Kedziora, G.; Khalliulin, R. Z.; Klunzinger, P.; Lee, A. M.; Lee, M. S.; Liang, W.; Lotan, I.; Nair, N.; Peters, B.; Proynov, E. I.; Pieniazek, P. A.; Min Rhee, Y.; Ritchie, J.; Rosta, E.; David Sherrill, C.; Simmonett, A. C.; Subotnik, J. E.; Lee Woodcock, H., III; Zhang, W.; Bell, A. T.; Chakraborty, A. K.; Chipman, D. M.; Keil, F. J.; Warshel, A.; Hehre, W. J.; Schaefer, H. F., III; Kong, J.; Krylov, A. I.; Gill, P. M. W.; Head-Gordon, M. *Phys. Chem. Chem. Phys.* **2006**, *8*, 3172-3191.
62. Hammett, L. P. *J. Am. Chem. Soc.* **1937**, *59*, 96-103.
63. Reiher, M.; Sundermann, A. *Eur. J. Inorg. Chem.* **2002**, 1854-1863.
64. McElvain, S. M.; Schroeder, J. P. *J. Am. Chem. Soc.* **1949**, *71*, 40-46.
65. Anastas, P.; Warner, J. *Green Chemistry: Theory and Practice*; Oxford University Press: Oxford, UK, 1998.
66. Akalay, D.; Durner, G.; Bats, J. W.; Bolte, M.; Gobel, M. W. *J. Org. Chem.* **2007**, *72*, 5618-5624.
67. Sheshenev, A. E.; Boltukhinam, E. V.; Grishina, A. A.; Cisarova, I.; Lyapkalo, I. M.; Hii, K. K. *Chem. -Eur. J.* **2013**, *19*, 8136-8143.
68. Dauer, D. -.; Stalke, D. *Dalton Trans.* **2014**, *43*, 14432-14439.

69. Viehe, H. G.; Janousek, Z. *Angew. Chem. Int. Ed.* **1973**, *12*, 806-818.
70. Schwindt, M. A.; Lejon, T.; Hegedus, L. S. *Organometallics* **1990**, *9*, 2814-2819.
71. Rogers, R. D.; Bynum, R. V.; Atwood, J. L. *J. Crystallogr. Spectrosc. Res.* **1984**, *14*, 29-34.
72. Shriver, D. F.; Drezdson, M. A. *The Manipulations of Air-Sensitive Compounds*; John Wiley & Sons: New York, USA, 1986.
73. Shaffer, D. W.; Ryken, S. A.; Zarkesh, R. A.; Heyduk, A. F. *Inorg. Chem.* **2011**, *50*, 13-21.
74. Giffin, N. A.; Hendsbee, A. D.; Masuda, J. D. *J. Organomet. Chem.* **2011**, *696*, 2533-2536.
75. Cremer, D.; Pople, J. A. *J. Am. Chem. Soc.* **1975**, *97*, 1354-1358.
76. Fulmer, G. R.; Miller, A. J. M.; Sherden, N. H.; Gottlieb, H. E.; Nudelman, A.; Stoltz, B. M.; Bercaw, J. E.; Goldberg, K. I. *Organometallics* **2010**, *29*, 2176-2179.
77. Kousksou, T.; Alaphilippe, M.; Jamil, A.; Rhafiki, T. E.; Mouqalid, M.; Zeraouli, Y. *Energy* **2014**, *66*, 919-926.
78. Bader, R. *Atoms in Molecules: A Quantum Theory*; Oxford University Press: Oxford, UK, 1990.
79. *The Quantum Theory of Atoms in Molecules*; Matta, C. F.; Boyd, R. J., Eds.; Wiley: Germany, 2007.
80. Wilson, E. E.; Oliver, A. G.; Hughes, R. P.; Ashfeld, B. L. *Organometallics* **2011**, *30*, 5214-5221.
81. Drouin, F.; Oguadinma, P. O.; Whitehorne, T. J. J.; Prud'homme, R. E.; Schaper, F. *Organometallics* **2010**, *29*, 2139-2147.

82. T. A. Keith. *AIMAll (Version 15.05.18)*, TK Gristmill Software: Overland Park, KS, USA, 2015 (aim.tkgristmill.com).
83. Vaughan, B. A.; Arsenault, E. M.; Chan, S. M.; Waterman, R. *J. Organomet. Chem.* **2012**, *696*, 4327-4331.
84. Vaughan, B. A.; Wetherby, A. E.; Waterman, R. *Acta Crystallogr., Sect. E: Struct. Rep. Online* **2012**, *E68*, m343.
85. Stewart, J. J. P. *J. Comput. Chem.* **1989**, *10*, 209-220.
86. Lee, C.; Yang, W.; Parr, R. G. *Phys. Rev. B* **1998**, *37*, 785-789.
87. Becke, A. D. *J. Chem. Phys.* **1993**, *98*, 5648-5652.
88. Moller, C.; Plesset, M. S. *Phys. Rev.* **1934**, *48*, 618-622.
89. Head-Gordon, M.; Pople, J. A. *Chem. Phys. Lett.* **1988**, *153*, 503-506.
90. M. J. Frisch, G. W. Trucks, H. B. Schlegel, G. E. Scuseria, M. A. Robb, J. R. Cheeseman, G. Scalmani, V. Barone, B. Mennucci, G. A. Petersson, H. Nakatsuji, M. Caricato, X. Li, H. P. Hratchian, A. F. Izmaylov, J. Bloino, G. Zheng, J. L. Sonnenberg, M. Hada, M. Ehara, K. Toyota, R. Fukuda, J. Hasegawa, M. Ishida, T. Nakajima, Y. Honda, O. Kitao, H. Nakai, T. Vreven, J. A. Montgomery Jr., J. E. Peralta, F. Ogliaro, M. Bearpark, J. J. Heyd, E. Brothers, K. N. Kudin, V. N. Staroverov, R. Kobayashi, J. Normand, K. Raghavachari, A. Rendell, J. C. Burant, S. S. Iyengar, J. Tomasi, M. Cossi, N. Rega, J. M. Millam, M. Klene, J. E. Knox, J. B. Cross, V. Bakken, C. Adamo, J. Jaramillo, R. Gomperts, R. E. Stratmann, O. Yazyev, A. J. Austin, R. Cammi, C. Pomelli, J. W. Ochterski, R. L. Martin, K. Morokuma, V. G. Zakrzewski, G. A. Voth, P. Salvador, J. J. Dannenberg, S. Dapprich, A. D. Daniels,

- O. Farkas, J. B. Foresman, J. V. Ortiz, J. Cioslowski and D. J. Fox. *Gaussian 09 Revision C.01*, Gaussian, Inc.: Wallingford, CT, 2009.
91. Zhao, Y.; Truhlar, D. G. *Theor. Chem. Acc.* **2008**, *120*, 215-241.
92. Chai, J. D.; Head-Gordon, M. *Phys. Chem. Chem. Phys.* **2008**, *10*, 6615-6620.
93. Macrae, C. F.; Bruno, I. J.; Chisholm, J. A.; Edgington, P. R.; McCabe, P.; Pidcock, E.; Rodriguez-Monge, L.; Taylor, R.; van de Streek, J.; Wood, P. A. *J. Appl. Crystallogr.* **2008**, *41*, 466-470.
94. *APEX II*, Bruker AXS Inc.: Madison, Wisconsin, USA, 2008.
95. *SAINT*, Bruker AXS Inc.: Madison, Wisconsin, USA, 2008.
96. *SADABS*, Bruker AXS Inc.: Madison, Wisconsin, USA, 2009.
97. Sheldrick, G. M. *Acta Cryst.* **2008**, *A64*, 112-122; *Acta Cryst.* **2015**, *A71*, 3-8; *Acta Cryst.* **2015**, *C71*, 3-8.
98. Spek, A. L. *Acta Cryst.* **2009**, *D65*, 148-155.

Chapter 6 – Appendix

6.1 Computational Data

Table A1: Energy output for the optimization of the R¹ position of the boron carbenoid at the B3LYP/6-31G* level of theory (R² = R³ = H).

R ¹	Singlet State Energy (Ha)	Triplet State Energy (Ha)	ΔE_{st} (Ha)	ΔE_{st} (kJ mol ⁻¹)
Mes	-949.62742	-949.634612	-0.007192	-18.882596
Dipp	-1185.490818	-1185.496559	-0.005741	-15.0729955
<i>t</i> -Bu	-566.136033	-566.138661	-0.002628	-6.899814
Ph	-713.734806	-713.737075	-0.002269	-5.9572595
<i>p</i> -tol	-792.370778	-792.37284	-0.002062	-5.413781

Table A2: Energy output for the optimization of the R² position of the boron carbenoid at the B3LYP/6-31G* level of theory (R¹ = R³ = H).

R ²	Singlet State Energy (Ha)	Triplet State Energy (Ha)	ΔE_{st} (Ha)	ΔE_{st} (kJ mol ⁻¹)
CF ₃	-925.702213	-925.715219	-0.013006	-34.147253
Ph	-713.754058	-713.764865	-0.010807	-28.3737785
Me	-330.267897	-330.275058	-0.007161	-18.8012055
NMe ₂	-519.573465	-519.568481	0.004984	13.085492
OMe	-480.682726	-480.674198	0.008528	22.390264
OEt	-559.318577	-559.309772	0.008805	23.1175275

Table A3: Summary of computed energy data for the optimized boron carbenoid by both DFT and Møller-Plesset methods using the 6-31G* basis set.

	B3LYP	MP2
Singlet State Energy (Ha)	-1100.045152	-1018.1304503962
Triplet State Energy (Ha)	-1100.039828	-1018.1164136363
ΔE_{st} (Ha)	0.005324	0.0140367599
ΔE_{st} (kJ mol ⁻¹)	13.978162	36.85351311745
Singlet State HOMO (eV)	-3.25	-5.43
Singlet State LUMO (eV)	-0.83	3.02
Singlet State HOMO-LUMO gap (eV)	2.42	8.45
Singlet State Dipole Moment (Debye)	5.29	9.33
ΔH_f {singlet carbenoid} (Ha)	-1099.59856	--
ΔH_f {dimer} (Ha)	-2199.31336	--
ΔG {singlet carbenoid} (Ha)	-1099.66689	--
ΔG {dimer} (Ha)	-2199.42102	--

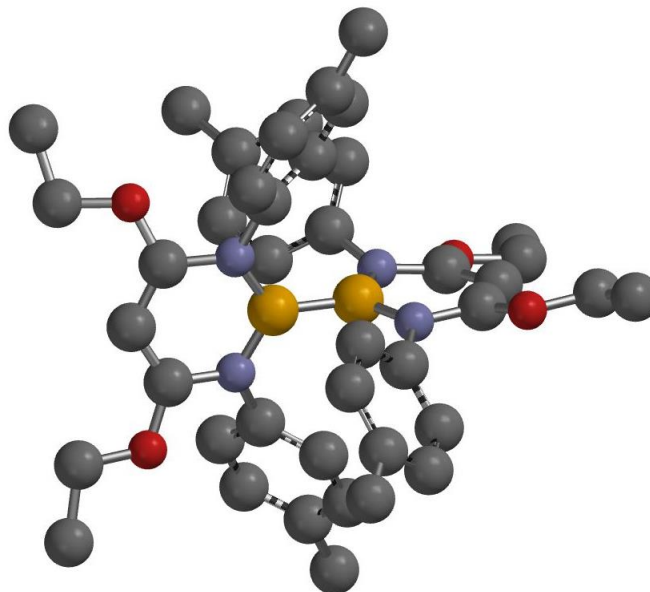


Figure A1: Graphical representation of **1d**, calculated at the B3LYP/6-31G* level of theory. Hydrogen atoms omitted for clarity. Calculated B–B bond length: 1.723 Å.

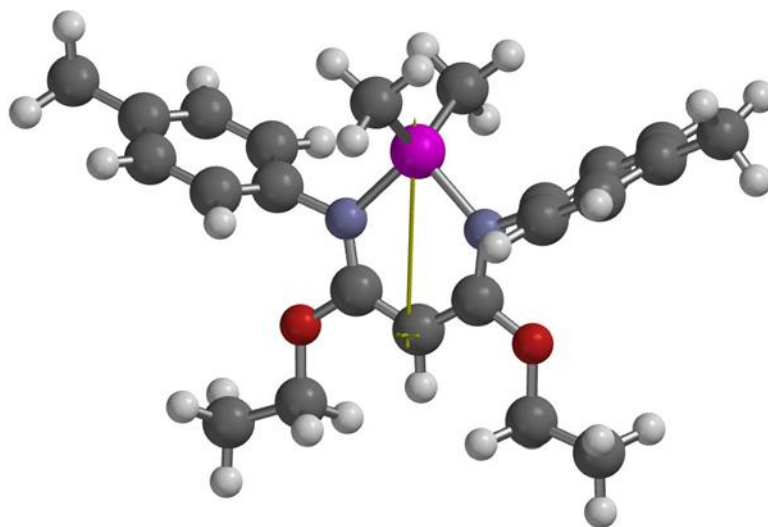


Figure A2: Graphical representation of the dipole in **6**, calculated at the B3LYP/6-31G* level of theory. The dipole vector is shown in yellow.

6.2 Crystallographic Data

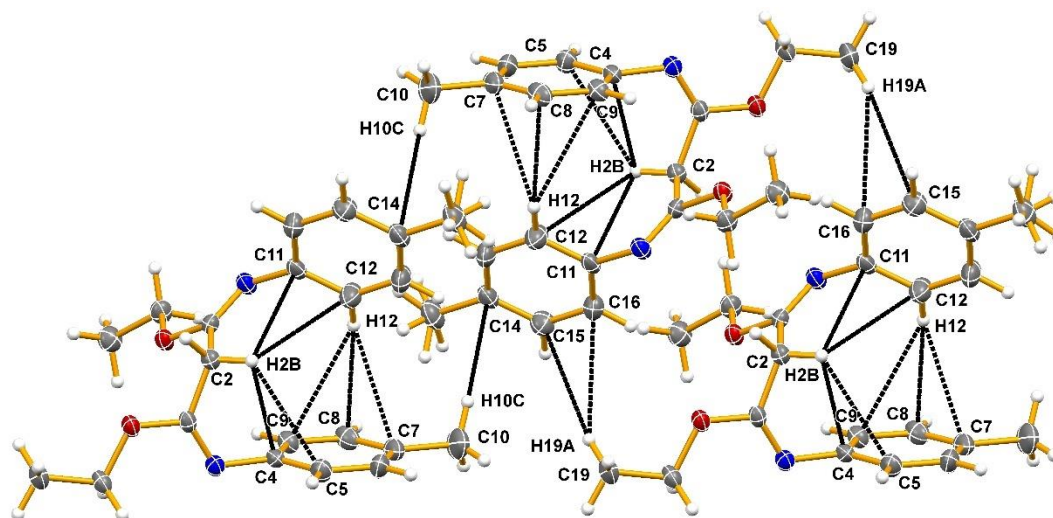


Figure A3: Ring contacts present in the solid state structure of **2**, showing the π -stacking interactions.



Figure A4: Large, “block-like” crystal of **6**, in the bottom of a 20 mL screw-cap vial (left), and in a weight-boat (right). The image on the left has been recoloured to “grayscale” for visual clarity.

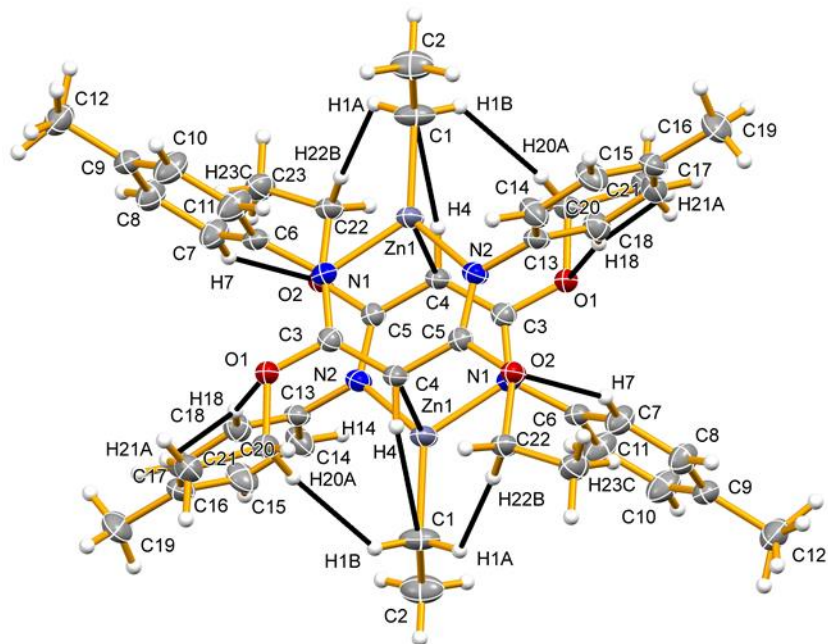


Figure A5: Solid state dimeric structure of **7**. Thermal ellipsoids are drawn at the 50% probability level.